Proc. Natl. Sci. Counc. ROC(A)
Vol. 18, No. 1, 1994. pp. 1-32

(Review Paper)

Airflow over Mesoscale Heat Sources Part I: Responses in a Uniform Flow

YUH-LANG LIN

Department of Marine, Earth, and Atmospheric Sciences
North Carolina State University
Raleigh, North Carolina 27695-8208, U.S.A.

(Received November 23, 1992; Accepted June 22, 1993)

ABSTRACT

The dynamics of mesoscale circulations of a stably stratified flow forced by both low-level and elevated heat sources or sinks is reviewed. The mathematical problems of prescribed diabatic heating in a continuously stratified flow have been solved by several authors and have been shown to be useful in understanding the dynamics of various mesoscale phenomena which commonly occur in the terrestrial atmosphere. In this paper, we review a relatively wider variety of problems and emphasize more the basic dynamics. In part I, we discuss the responses of a stably stratified uniform flow to a prescribed thermal forcing. The governing equations, energy equation, momentum transport, dispersion relation, and various wave regimes and properties are discussed. Mathematical methods for solving both steady and transient flows over a meso-γ scale heat source are presented. The applications of the mathematical solutions to problems of heat island, orographic rain, moist convection, and gravity waves traveling on inversions are also discussed.

Key Words: mesoscale circulation, diabatic heating, meso-γ scale, pulse heating, steady heating, heat island, orographic rain, moist convection, gravity waves

I. Introduction

There are a number of problems in mesoscale dynamics which are related to the response of a stably stratified flow to localized heat sources or sinks. A phenomenon is defined as mesoscale if it has a horizontal scale of 2 to 2000 km. The mesoscale is often divided into three subscales: meso-γ (2-20 km), meso-β (20-200 km), and meso-α (200-2000 km) scales (Orlanski, 1975). In some cases, the diabatic heating or cooling reaches a quasi-steady state, which may be represented by a prescribed function. In this way, the mathematical problem reduces to a stably stratified flow over a prescribed thermal forcing. Some examples will be briefly reviewed below to demonstrate that this type of study is useful in understanding the dynamics of different types of mesoscale phenomena spanning the various subscales.

One of the earliest theoretical studies of airflow over a prescribed heat source was proposed by Malkus and Stern (1953) in a study of the heat island problem. They found that the air ascends over the heat island. As pointed out by Olfe and Lee (1971) and Smith and Lin (1982), this is not the case if a correct upper boundary condition is imposed. Observations over heat islands such as Anegada (Malkus, 1963) and Barbados (Fig. 22; DeSouza, 1972; summarized in Garstang *et al.*, 1975) showed that there exists a region of descent over the heat island, followed by an ascent over the ocean on the downwind side during the daytime. By solving an associated transient problem, Lin and Smith (1986) also suggested that the rainfall enhancement occurring on the downwind side of an urban heat island, such as in St. Louis (Fig. 1; Braham and Dungey, 1978; Changnon, 1981), may be partly the result of the ascent produced by stationary heating due to the urban heat island. This problem has also been studied by several authors (e.g. Smith, 1955, 1957; Hsu, 1987a, b; Luthi *et al.*, 1989). Circulations associated with sea/land breezes are also related to this process except that the thermal forcing is periodic in time. Since the sea breeze problem has been studied extensively in the last four decades and is reviewed in several textbooks and literature articles (e.g., Rotunno, 1983), we will not review this subject in this paper.

In a study of the upslope orographic rain problem, Smith and Lin (1982) solved the mathematical problem analytically using a prescribed function to represent the latent heating associated with the nonprecipitating or precipitating orographic cloud in a

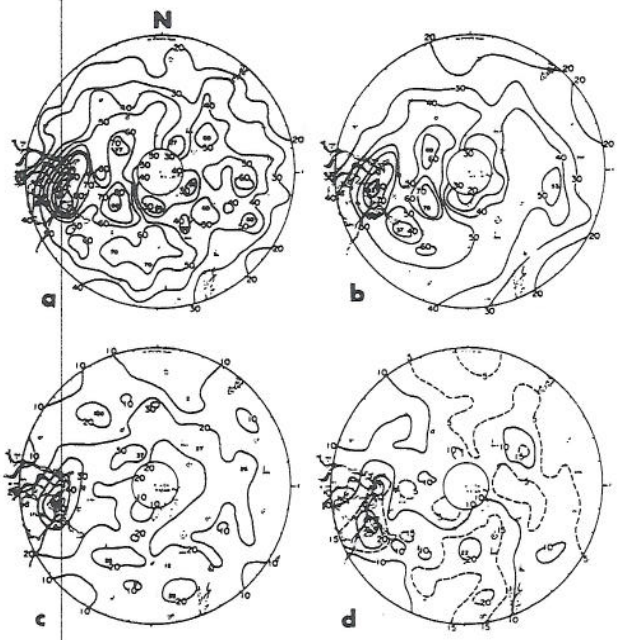

Fig. 1. Maps of first echo densities in St. Louis, Mo.: (a) analysis of 4553 first echoes, (b) set of 4175 first echoes having bases ≥ 3000 ft, (c) set of 1950 echoes from 44 days selected to insure ground based convective clouds, (d) data for days with light wind. Downtown St. Louis is denoted by *X*. Notice that the first echo formation is on the downwind region of the city. (From Braham and Dungey, 1978)

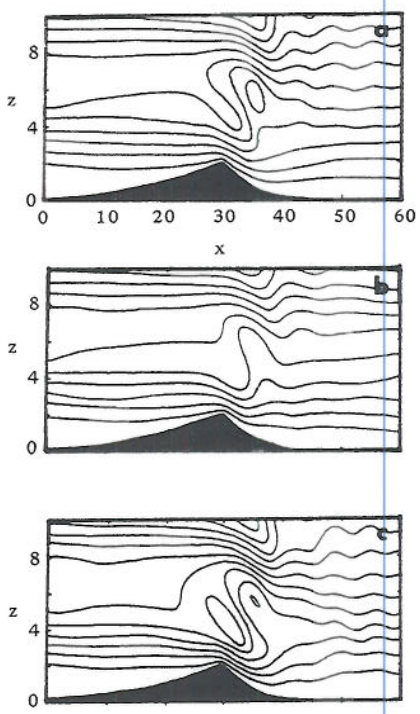

Fig. 2. Airflow over a ridge: (a) adiabatic, (b) with boundary layer heating, and (c) with boundary layer cooling. Notice that the adiabatic mountain waves are suppressed by the heating and enhanced by the cooling. (From Raymond, 1972)

stably stratified flow. They found that the phase relationship between the heating and the induced vertical displacement is negative in a moving airstream. That is, descending motion is established just upstream of the prescribed heated region so that negative displacements dominate in the heating region. This phenomenon is consistent with other studies of the orographic rain problem (e.g., Fraser *et al.*, 1973; Barcilon *et al.*, 1980), in which it was found that mountain waves are weakened by latent heating. Raymond (1972) also showed that mountain waves are weakened by heating and strengthened by cooling in a study of airflow over a two-dimensional ridge with low-level sensible heating and cooling (Fig. 2). This phenomenon was then explained by Lin and Smith (1986) by solving the transient problem and by Bretherton (1988) by proposing a group velocity argument. The combined effect of thermal and orographic forcing has also been studied by Davies and Schar (1986). In their theory, they incorporated a CISK-like representation for a non-precipitating convective cloud in a linear, steady, continuously stratified, hydrostatic flow over a mountain ridge. They found that the effect of combined thermal and orographic forcing can be significantly different from that of orography acting alone. In particular, in certain situations an enhanced (resonant) response can occur with strong winds on the lee slope and a concomitant large surface pressure drag. Their results also suggested that diabatic effects might on occasion play a major role in inducing strong surface leeside winds.

The response of a continuously stratified atmosphere to diabatic forcing is also relevant to the moist convection associated with midlatitude squall lines. One may regard the evaporative cooling in the subcloud layer produced by the precipitation falling from the updraft aloft as a stationary heat sink in the reference frame of the moving line. The steady state assumption for the cooling in squall-line type thunderstorms is not an unreasonable one (Lilly, 1979). The mathematical problem has been investigated by several authors (Thorpe *et al.*, 1980; Lin and Smith, 1986; Raymond and Rotunno, 1989; Lin and Chun, 1991). The solutions provide a way to help explain the maintenance of a long lasting squall line. In solving a similar two-dimensional initial value problem with both prescribed condensational heating and evaporative cooling considered, Raymond (1986) indicated that the strong speed selectivity of wave-CISK is due to the requirement that the actual vertical velocity at the level of free convection exceed the diabatic mass flux there. In solving the three-di-

mensional response to a prescribed elevated heating, representing condensational heating, Lin (1986a) and Lin and Li (1988) proposed that the V-shaped cloud tops over severe storms (Fig. 3; also see Heymsfield and Blackmer, 1988 for a brief review) are formed by thermally forced gravity waves. By incorporating a prescribed elevated cooling associated with melting snow, it has been shown that new convection may be triggered (Lin *et al.*, 1988a, b).

Therefore, the mathematical problem of prescribed diabatic heating in a continuously stratified flow has been shown to be useful in understanding the dynamics of various mesoscale phenomena which commonly occur in the terrestrial atmosphere by the above authors and by others. This subject has been reviewed recently by Lin and Stewart (1991). However, we will review a wider variety of problems and place more emphasis on the basic dynamics. The governing equations for a mesoscale atmospheric system will be presented in Section II. An energy equation will be used to identify various instability mechanisms. A dispersion relation will be derived and used to categorize different wave regimes. Finally, the wave reflection and effect of critical level will be discussed. In Section III, the response of a uniform, steady, continuously stratified flow over a meso-γ scale heat source or sink will be described. Both sinusoidal and isolated heat sources will be considered. Applications to the orographic rain

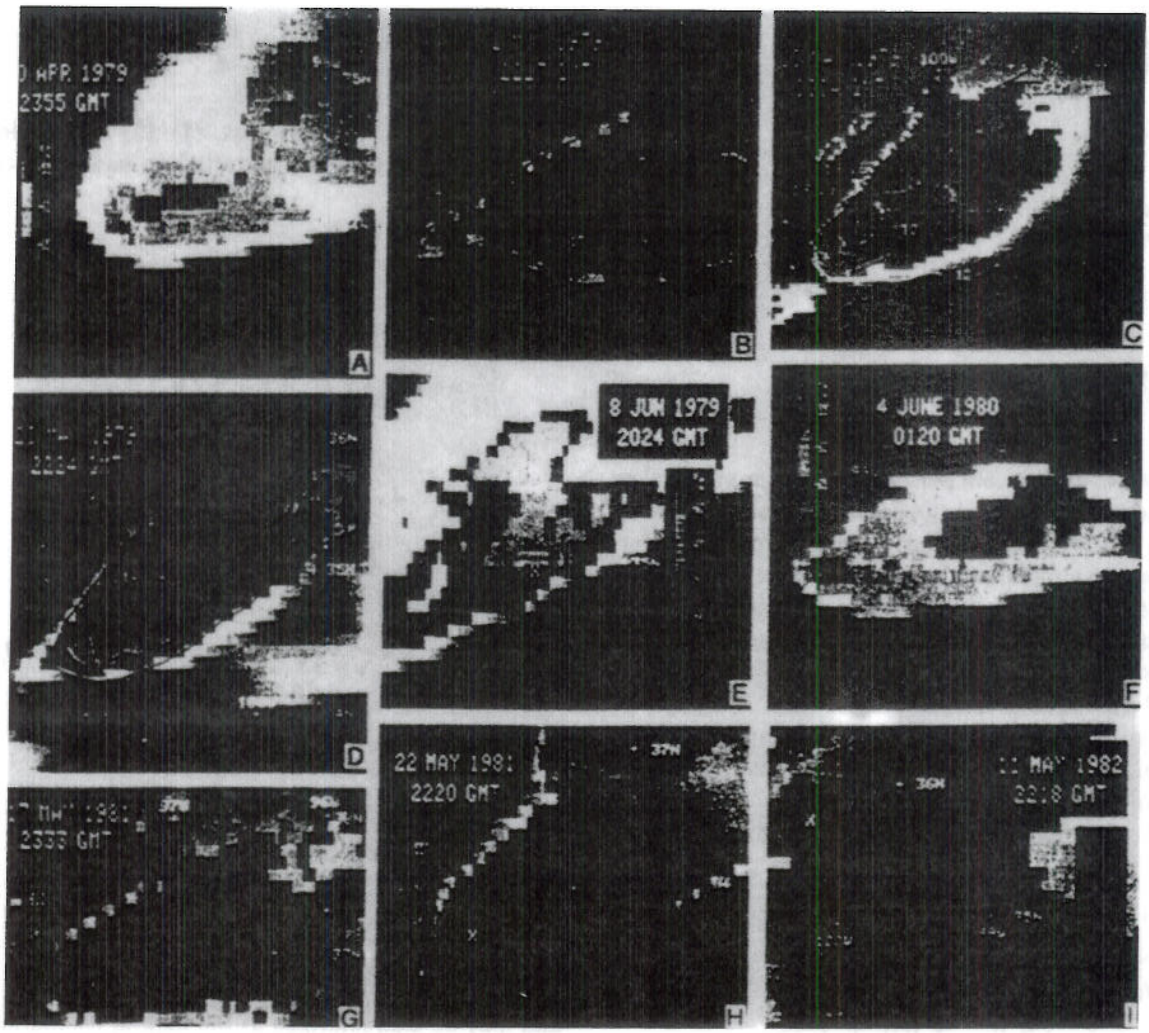

Fig. 3. IR GOES images. Stereo height contours are shown when available; an *X* indicates approximate cloud top position as obtained from the visible image. Note that the *V*-shaped cloud tops formed over severe storms for different cases (From Heymsfield and Blackmer, 1988).

problem will be discussed. In Section IV, the transient flow response to a meso-γ scale heat source will be reviewed. Both pulse heating and steady heating will be included. Applications to mesoscale circulations induced by orographic rain, heat islands, moist con vection and gravity waves on inversions will be reviewed.

II. Governing Equations of Mesoscale Systems

Consider an inviscid, incompressible atmosphere on a planetary f-plane. The momentum equations, the incompressible continuity equation, and the thermodynamic energy equation can be expressed in the form (e.g., Smith, 1979; Emanuel and Raymond, 1984)

$$\frac{Du}{Dt} - fv + \frac{1}{\rho}\frac{\partial p}{\partial x} = 0 \tag{1}$$

$$\frac{Dv}{Dt} + fu + \frac{1}{\rho}\frac{\partial p}{\partial y} = 0 \tag{2}$$

$$\frac{Dw}{Dt} + g + \frac{1}{\rho}\frac{\partial p}{\partial z} = 0 \tag{3}$$

$$\frac{\partial u}{\partial x} + \frac{\partial v}{\partial y} + \frac{\partial w}{\partial z} = 0 \tag{4}$$

$$\frac{D\theta}{Dt} = \frac{\theta_o}{c_p T_o} q . \tag{5}$$

The diabatic heating rate per unit mass, q, may be taken to represent the surface heating and/or the elevated latent heating. The symbols θ_o and T_o denote constant reference potential temperature and temperature, respectively. Other symbols are defined as usual. Notice that the Rayleigh friction and Newtonian cooling may be included to generalize the above system. Since we have assumed an incompressible atmosphere, the physical mechanism responsible for generation and subsequent propagation of sound (acoustic) waves has been eliminated from the system.

We may linearize the above system by defining

$$\begin{aligned}
u(t, x, y, z) &= U(z) + u'(t, x, y, z) \\
v(t, x, y, z) &= V(z) + v'(t, x, y, z) \\
w(t, x, y, z) &= \quad\; w'(t, x, y, z) \\
\rho(t, x, y, z) &= \rho_o + \rho'(t, x, y, z) \\
p(t, x, y, z) &= p(x, y, z) + p'(t, x, y, z) \\
\theta(t, x, y, z) &= \Theta(x, y, z) + \theta'(t, x, y, z) \\
q(t, x, y, z) &= \quad\; q'(t, x, y, z)
\end{aligned} \tag{6}$$

In the above expressions, the Boussinesq approximation (Spiegel and Veronis, 1960) has been adopted, which assumes the density to be constant except in the buoyancy term. The basic wind is constrained to be uniformly horizontal. The basic state momentum relations are assumed to satisfy the hydrostatic and geostrophic wind balance

$$\frac{\partial P}{\partial z} = -g\rho_o \tag{7a}$$

$$U = \frac{-1}{f\rho_o}\frac{\partial P}{\partial y}, \quad V = \frac{1}{f\rho_o}\frac{\partial P}{\partial x} . \tag{7b}$$

The above equations imply the existence of thermal wind balance for the basic state

$$\frac{\partial \Theta}{\partial x} = \frac{f\theta_o}{g} V_z , \quad \frac{\partial \Theta}{\partial y} = -\frac{f\theta_o}{g} U_z . \tag{8}$$

Substituting Eq. (6) into Eqs. (1)–(5) and neglecting the nonlinear terms, the perturbation equations can be written as

$$\frac{\partial u'}{\partial t} + U\frac{\partial u'}{\partial x} + V\frac{\partial u'}{\partial y} + U_z w' - fv' + \frac{1}{\rho_o}\frac{\partial p'}{\partial x} = 0 \tag{9}$$

$$\frac{\partial v'}{\partial t} + U\frac{\partial v'}{\partial x} + V\frac{\partial v'}{\partial y} + V_z w' + fu' + \frac{1}{\rho_o}\frac{\partial p'}{\partial y} = 0 \tag{10}$$

$$\frac{\partial w'}{\partial t} + U\frac{\partial w'}{\partial x} + V\frac{\partial w'}{\partial y} - g\frac{\theta'}{\theta_o} + \frac{1}{\rho_o}\frac{\partial p'}{\partial z} = 0 \tag{11}$$

$$\frac{\partial u'}{\partial x} + \frac{\partial v'}{\partial y} + \frac{\partial w'}{\partial z} = 0 \tag{12}$$

$$\frac{\partial \theta'}{\partial t} + U\frac{\partial \theta'}{\partial x} + V\frac{\partial \theta'}{\partial y} + \frac{f\theta_o}{g}(V_z u' - U_z v') + \frac{N^2\theta_o}{g} w'$$

$$= \frac{\theta_o}{c_p T_o} q' . \tag{13}$$

The Brunt-Vaisala frequency is defined as

$$N^2 = \frac{g}{\theta_o}\frac{\partial \Theta}{\partial z} \tag{14}$$

and may be characterized as the natural oscillation frequency of an air parcel displaced from its equilibrium positions in a continuously stratified atmosphere.

Equations (9)–(13) can be combined to give a single equation for the vertical velocity:

$$\frac{D}{Dt}\{\frac{D^2}{Dt^2}\nabla^2 w' + f^2 w'_{zz} - (U_{zz}\frac{D}{Dt} + f V_{zz}) w'_x$$

$$-(V_{zz}\frac{D}{Dt} - f U_{zz}) w'_y + N^2 \nabla_H^2 w'$$

$$+2f(U_z w'_{yz} - V_z w'_{xz})\} + 2f U_z V_z (w'_{xx} - w'_{yy})$$

$$+2f(V_z^2 - U_z^2) w'_{xy} - 2f^2 (U_z w'_{xz} + V_z w'_{yz})$$

$$= \frac{g}{c_p T_o}\frac{D}{Dt}\nabla_H^2 q' . \qquad (15)$$

The above mesoscale system includes the following mechanisms: (a) inertia-gravity wave generation, (b) convective instability, (c) shear instability, (d) symmetric instability, and (e) baroclinic instability (Emanuel and Raymond, 1984).

The energy transfer equation for the system of Eqs. (9)–(13) with no north-south (meridional) basic state wind component (V=0) but including the meridionally sheared zonal flow ($U_y \neq 0$) can be derived as

$$(\frac{\partial}{\partial t} + U\frac{\partial}{\partial x})E + \rho_o u' w' U_z + \rho_o u' v' U_y$$

$$-\frac{\rho_o g f}{N^2 \theta_o} v' \theta' U_z + \nabla \cdot (p' V') = (\frac{\rho_o g^2}{c_p T_o N^2 \theta_o}) \theta' q' , \qquad (16)$$

where

$$E = \frac{\rho_o}{2}[(u'^2 + v'^2 + w'^2) + (\frac{g}{N\theta_o})^2 \theta'^2] \qquad (17)$$

is the total perturbation energy, which consists of the perturbation kinetic energy (first term) and the perturbation potential energy (second term). Taking the horizontal integration of Eq. (17) over a single wavelength for a periodic disturbance or from -∞ to +∞ for a localized disturbance in both x and y directions gives

$$\frac{\partial \bar{E}}{\partial t} = -\rho_o \overline{u w} U_z - \rho_o \overline{u v} U_y + (\frac{\rho_o g f}{N^2 \theta_o}) \overline{v \theta} U_z - \frac{\partial}{\partial z}\overline{p w}$$

$$+(\frac{\rho_o g^2}{c_p T_o N^2 \theta_o}) \overline{\theta q} . \qquad (18)$$

Now we may take the vertical integration of the above equation from z=0 to the top of the physical domain z=z_T in which we are interested, to yield

$$\frac{\partial E_T}{\partial t} = -\rho_o \int_0^{z_T} \overline{u w} U_z dz - \rho_o \int_0^{z_T} \overline{u v} U_y dz + (\frac{\rho_o g f}{N^2 \theta_o})$$

$$\cdot \int_0^{z_T} \overline{v \theta} U_z dz - \overline{p w}(z_T) + \overline{p w}(0)$$

$$+(\frac{\rho_o g^2}{c_p T_o N^2 \theta_o}) \int_0^{z_T} \overline{\theta q} dz , \qquad (19)$$

where E_T is the domain-integrated E.

The term on the left side of the above equation represents the time rate of change in the total perturbation energy in the system. The first term on the right side represents the vertical momentum flux transfer between the kinetic energy of the basic current and the wave energy. When shear instability occurs, the energy is transferred from the basic state shear flow to the disturbance, resulting in a net loss of kinetic energy of the basic state. The second term on the right side represents the horizontal momentum flux transfer between the kinetic energy of the basic current and the wave energy. When inertial instability occurs, the perturbation grows by extracting the kinetic energy from the horizontal basic shear. The third term on the right side represents the north-south heat flux transfer between the basic state and the perturbations. When baroclinic instability occurs, the perturbation extracts energy from the vertical shear, which is supported by the northward heat flux. The fourth term represents the forcing exerted by the top boundary. It is zero if the top boundary is a flat rigid surface because that physical condition constrains w'=0 there. This term becomes negative if a radiation upper boundary condition is applied, which requires the energy generated below to propagate upward from the domain interested. The fifth term represents the forcing exerted by the lower boundary. It is zero if the lower boundary is a flat rigid boundary and positive if there exists irregular topography (e.g., a mountain). The last term on the right side of the above equation represents the energy transfer due to thermal forcing. In order for the disturbance to grow, the diabatic heating has to be added where the potential temperature anomaly is positive. That is, the heat should be added in the warm region. When static or buoyant instability occurs, the N^2 term of the total perturbation engrgy becomes negative. Thus, the energy is transferred from the potential energy (N^2 term) to the kinetic energy.

In this paper, we will focus on the physical characteristics of wave generation in a stably straitified fluid applicable to thermally forced mesoscale circulations in planetary atmospheres. Therefore, we will review the basic properties of inertia-gravity wave generation in the following. Those readers interested in other generation mechanisms should consult the various review papers which exist in the literature or standard texts on the subject.

For simplicity, we consider an adiabatic linear system with constant U, N, and f. Under this situation, Eq. (15) reduces to

$$(\frac{\partial}{\partial t}+U\frac{\partial}{\partial x})^2(\frac{\partial^2 w'}{\partial x^2}+\frac{\partial^2 w'}{\partial y^2}+\frac{\partial^2 w'}{\partial z^2})+f^2\frac{\partial^2 w'}{\partial z^2}$$

$$+N^2(\frac{\partial^2 w'}{\partial x^2}+\frac{\partial^2 w'}{\partial y^2})=0. \qquad (20)$$

Assume a wave-like solution for w'

$$w'=\hat{w}(z)\exp[i(kx+ly-\omega t)]. \qquad (21)$$

Substituting (21) into (20) gives

$$\frac{\partial^2 \hat{w}}{\partial z^2}+\lambda^2\hat{w}=0, \qquad (22)$$

where

$$\lambda^2=\frac{\kappa^2(N^2-\Omega^2)}{\Omega^2-f^2}. \qquad (23)$$

κ is the horizontal wave number, $(k^2+l^2)^{1/2}$, and Ω is defined to be the Doppler-shifted or intrinsic frequency, ω-kU. The solution of Eq. (22) can be written as

$$\hat{w}\sim e^{\pm i\lambda z}. \qquad (24)$$

Therefore, the wave property depends on the values of λ. Three different wave regimes can be identified and defined from the signs of the numerator and denominator of Eq. (23).

(1) $\Omega > N > f$: In this wave regime, λ is imaginary. Disturbances decay exponentially with height away from the source. Thus, the wave falls into the *evanescent wave regime*. When $\Omega >> N > f$, Eq. (23) reduces to

$$\lambda^2 \mathrm{E} -\kappa^2.$$

In this extreme case, the buoyancy and rotational forces play insignificant roles in the wave generation. The fluid behaves like a *homogeneous fluid*, and the flow field may be adquately characterized as one on *potential flow*. An extensive mathematical theory exists to describe flows of this type (e.g., Lamb, 1932).

(2) $N > \Omega > f$: In this wave regime, λ is real, and the wave is able to propagate freely in the vertical. Thus, the wave falls into the *vertically propagating wave regime*. One of the two possible mathematical solutions of Eq. (24) represents a wave propagating upward, while the other represents a wave propagating downward. For a wave generated by a low-level source such as a mountain, the Sommerfeld radiation condition requires the wave to propagate away from the energy source (i.e., upward from the mountain terrain). The other solution has no physical basis and is not retained. This also applies to the boundary condition at $z=+\infty$ for an elevated thermal forcing. However, both solutions of Eq. (24) must be retained in the heating layer (forcing region) and the layer between the heating base and the lower boundary (planetary surface). Since N/f typically is large in the atmosphere and the ocean, this wave regime is applicable to a wide range of intrinsic frequencies. When $N > \Omega >> f$ and $O(N) = O(\Omega)$, Eq. (23) reduces to

$$\lambda^2 \mathrm{E} \kappa^2(\frac{N^2}{\Omega^2}-1).$$

In this limit, the rotational effect may be ignored and the flow approaches the *nonhydrostatic wave regime*. When $N >> \Omega >> f$, Eq. (23) reduces to

$$\lambda^2 \mathrm{E}(\frac{\kappa N}{\Omega})^2.$$

For this case, the wave generation can be adquately determined by neglecting both the vertical acceleration and the rotational effects. Thus, the wave falls into the *nonrotating hydrostatic wave regime*. When $N >> \Omega > f$ and $O(\Omega) = O(f)$, Eq. (23) reduces to

$$\lambda^2 \mathrm{E}\frac{\kappa^2 N^2}{\Omega^2-f^2}.$$

In this limit, the vertical acceleration may be neglected in comparison with the buoyancy acceleration. Therefore, the flow approaches a hydrostatic balance, and the wave falls into the *rotating hydrostatic regime*. For the case with $N > \Omega >> f$, the rotational effect can be neglected. Therefore, the wave falls into the *pure gravity wave regime*.

(3) $N > f > \Omega$: In this wave regime, λ is imaginary. Similar to the first case, disturbances decay exponentially with height away from the source. Thus, the wave falls into the *evanescent wave regime*. However, the wave frequency is low. When $N > f >> \Omega$, the inertial terms, i.e. acceleration terms, play minor roles

in the wave generation. The flow is characterized as being *quasi-geostrophic*. In this wave regime, the fluid motion is nearly horizontal.

From the incompressible continuity equation, it can be shown that inertia-gravity waves are transverse to the flow. That is, the fluid particle motion is perpendicular to the wave vector. In addition, the velocity vector associated with a plane inertia-gravity wave rotates anticyclonically with time. The projection of the motion on the horizontal plane is an ellipse with ω/f as the ratio of major and minor axes.

Since the wave energy propagates with the group velocity, it is important to discuss the group velocity of inertia-gravity waves. Assuming the vertical eigenfunctions to be of the form $\hat{w}(z)\sim\exp(imz)$ and substituting into Eq. (22) yields the dispersion relation for inertia-gravity waves in a quiescent (motionless basic state), continuously stratified fluid:

$$\omega^2=\frac{f^2m^2+\kappa^2N^2}{k^2+l^2+m^2}. \tag{25}$$

The group velocity for inertia-gravity waves can be found by taking the derivatives of the frequency with respect to wavenumber, i.e.

$$c_{gx}=\partial\omega/\partial k,\quad c_{gy}=\partial\omega/\partial l,\quad c_{gz}=\partial\omega/\partial m. \tag{26}$$

Applying the above definitions to the dispersion relation for inertia-gravity waves, Eq. (25), gives

$$c_{gx}=\frac{km^2(N^2-f^2)}{(k^2+l^2+m^2)^{3/2}(f^2m^2+\kappa^2N^2)^{1/2}}, \tag{27a}$$

$$c_{gy}=\frac{lm^2(N^2-f^2)}{(k^2+l^2+m^2)^{3/2}(f^2m^2+\kappa^2N^2)^{1/2}}, \tag{27b}$$

$$c_{gz}=\frac{-m\kappa^2(N^2-f^2)}{(k^2+l^2+m^2)^{3/2}(f^2m^2+\kappa^2N^2)^{1/2}}. \tag{27c}$$

It can be shown that

$$\boldsymbol{c}_g\cdot\boldsymbol{k}=0, \tag{28}$$

where $\boldsymbol{k}=(k, l, m)$ is the wave vector. Thus, the group velocity vector for inertia-gravity waves is perpendicular to the wave vector.

One of the more important phenomena associated with gravity waves is wave reflection. If the basic atmospheric structures, such as the Brunt-Vaisala frequency and the basic wind speed, are allowed to vary with height, then the gravity wave may be reflected from the interface at which a rapid change of the basic atmospheric structure occurs. Consider small-amplitude perturbations in a two-dimensional nonrotating system governed by the set of Eqs. (22) and (23) but whose basic state is generalized to allow the basic wind and Brunt-Vaisala frequency to vary with height. The governing equation for $\hat{w}$ may be written as

$$\frac{\partial^2\hat{w}}{\partial z^2}+\lambda^2(z)\hat{w}=0, \tag{29}$$

where

$$\lambda^2(z)=\frac{1}{c-U}\frac{d^2U}{dz^2}+\frac{N^2}{(c-U)^2}-k^2. \tag{30}$$

The above equation is a simplified version of the Taylor-Goldstein equation, which was first derived independently by Taylor (1931) and Goldstein (1931). As discussed above, the solution of Eq. (29) is of the form $\exp(\pm i\lambda z)$. If λ^2 changes sign from positive to negative at a certain level, then λ will change from being a real to an imaginary number. This indicates a transition from the vertically propagating wave regime to the evanescent wave regime. Therefore, if a wave-like disturbance exists below that particular level, it will decay exponentially above that level. Under this situation, the wave energy is not able to propagate vertically above that particular level freely and is forced to reflect back from there. Therefore, this level is called the *wave reflection level*. If there exists such a level above the rigid (lower) surface, this atmospheric layer then acts as a waveguide trapping the wave energy between the reflection level and the surface and allows for effective far downstream propagation of the wave energy. One well-known example of gravity wave reflection are the lee waves generated by stratified flow over a mountain range.

Another important phenomenon associated with gravity waves is the change of wave property in passing through a critical level. A critical level (z_c) is defined as the level at which the vertically sheared basic flow $U(z)$ is equal to the horizontal phase speed (c), i.e. $U(z_c)=c$. Using the WKB method, Bretherton (1966) showed that an upward propagating internal wave packet would approach the critical layer for the dominant frequency and wavenumber of the packet. However, it would not reach the critical layer in any finite time since along a ray path, $dz/dt\propto(z-z_c)^2$ as $z\rightarrow z_c$, which gives $t-t_o\propto 1/(z-z_c)$ as $z\rightarrow z_c$. This means that it would take an infinite amount of time for the wave packet to reach the critical level. Thus, Bretherton inferred that the internal wave would be physically absorbed at the critical level, instead of being transmitted or reflected.

Mathematically, the governing equation (29) becomes singular at $z=z_c$. To discuss the wave properties near the critical level, we follow the study of Booker and Bretherton (1967) and the review of LeBlond and Mysak (1978). These authors used the method of Frobenius (e.g., see Hildebrand, 1976) in order to extract information about the wave behavior near the critical level. Notice that the WKB method is not valid near the critical level since it requires a large Richardson number (N^2/U_z^2).

At $z=z_c$, U and N may be expanded in a power series:

$$U = c + U_{zc}(z-z_c) + \cdots$$
$$N = N_c + N_{zc}(z-z_c) + \cdots, \tag{31}$$

where the subscript c denotes the value at the critical level. We assume that z_c is a regular singularity which requires $U_{zc} \neq 0$. A series solution may be found near z_c (carets are dropped):

$$w(z) \equiv A(z-z_c)^{1/2+i\mu} + B(z-z_c)^{1/2-i\mu}$$
$$= A\exp[(\tfrac{1}{2}+i\mu)(\ln|z-z_c|+i\arg(z-z_c)]$$
$$+ B\exp[(\tfrac{1}{2}-i\mu)(\ln|z-z_c|+i\arg(z-z_c)]$$
$$\equiv w_A + w_B. \tag{32}$$

Both w_A and w_B have a branch point at $z=z_c$. For the sake of definiteness, we may choose that branch of the ln function for which $\arg(z-z_c)=0$ when $z>z_c$ and introduce the branch cut from $z=z_c$ along the negative x-axis. Therefore, we obtain

$$w_A^+ = A\sqrt{|z-z_c|}\exp[i\mu\ln(z-z_c)]$$
$$w_B^+ = B\sqrt{|z-z_c|}\exp[-i\mu\ln(z-z_c)] \quad \text{for } z > z_c \tag{33}$$

As $z-z_c$ decreases continuously from positive to negative values, $\arg(z-z_c)$ can change continuously from 0 to π or 0 to $-\pi$. To determine the argument, we may add a small Rayleigh friction with a positive coefficient ν. The term $U-c$ then becomes $U - c - ic_i$, where $c_i = \nu k$. This lifts the z_c to be above the branch cut for $U_{zc} > 0$, which corresponds to the contour in the lower half plane under the branch cut in an inviscid flow (Fig. 4). That is, $\arg(z-z_c)$ changes from 0 to $-\pi$ for $U_{zc} > 0$. Thus, we must choose $\arg(z-z_c) = -\pi\,\mathrm{sgn}\,U_{zc}$ when $z < z_c$. Substituting this into Eq. (32) yields

$$w_A^- = A\sqrt{|z-z_c|}\exp[i\mu\ln(z-z_c) - (1/2)\pi i \cdot \mathrm{sgn}\,U_{zc} + \mu\pi\,\mathrm{sgn}\,U_{zc}]$$
$$w_B^- = B\sqrt{|z-z_c|}\exp[-i\mu\ln(z-z_c) - (1/2)\pi i \cdot \mathrm{sgn}\,U_{zc} - \mu\pi\,\mathrm{sgn}\,U_{zc}] \quad \text{for } z < z_c. \tag{34}$$

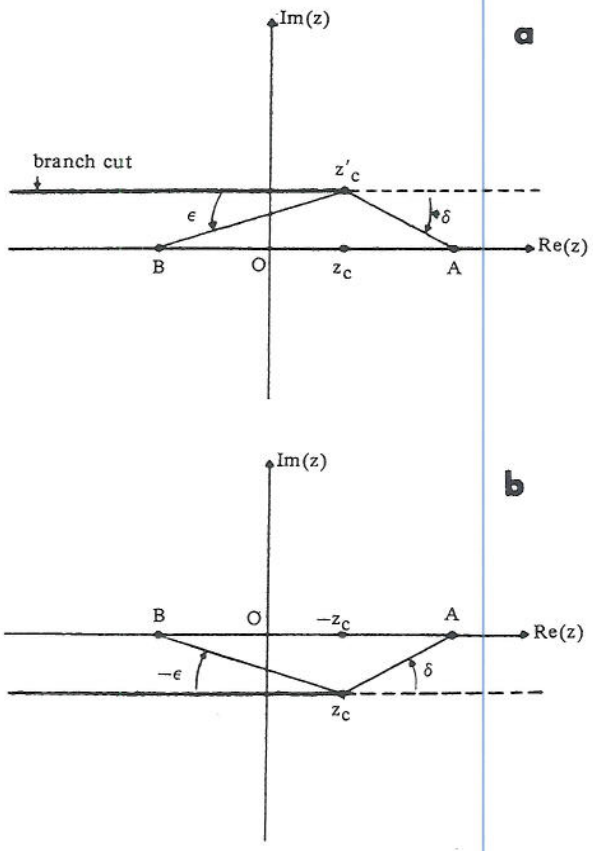

Fig. 4. Location of branch point with Rayleigh friction included for $z_c > 0$, (a) $U_{zc} > 0$; (b) $U_{zc} < 01$. (From LeBlond and Mysak, 1978)

Both solutions w_A and w_B satisfy the governing equation mathematically. From Eqs. (33) and (34), we have

$$\left|\frac{w_A^+}{w_A^-}\right| = \exp(-\mu\pi\,\mathrm{sgn}\,U_{zc}), \quad \left|\frac{w_B^+}{w_B^-}\right| = \exp(\mu\pi\,\mathrm{sgn}\,U_{zc}). \tag{35}$$

For $U_{zc} > 0$ and a low-level forcing, the amplitude of the disturbance generated in the lower level should decrease as it crosses the critical level to the upper layer. Thus, we must choose w_A. The proper solution can be found for other situations as well. Notice that the above equation also indicates that the wave energy is attenuated exponentially through the critical level as pointed out by Booker and Bretherton (1967). In addition, the vertical wavenumber becomes larger, and the perturbation velocity becomes more and more hori-

zontal as one approaches the critical level since

$$\lambda^2(z) \approx \frac{N^2}{(c-U)^2}. \tag{36}$$

This implies that $\lambda \to \infty$ as $z \to z_c$. Thus, the vertical wavelength approaches zero (Fig. 5).

III. Steady Flow over a Meso-γ Scale Heat Source

1. Sinusoidal Heat Source

For a uniform, steady, inviscid flow over a two-dimensional meso-γ scale heat source, the Rossby number is high, and the effects due to planetary rotation can be ignored. Notice that the meso-γ scale is defined to be the horizontal scale from 2 to 20 km (Orlanski, 1975). With these assumptions, Eqs. (9)–(13) can be reduced to

$$U\frac{\partial u'}{\partial x} + \frac{1}{\rho_o}\frac{\partial p'}{\partial x} = 0 \tag{37}$$

$$U\frac{\partial w'}{\partial x} - g\frac{\theta'}{\theta_o} + \frac{1}{\rho_o}\frac{\partial p'}{\partial z} = 0 \tag{38}$$

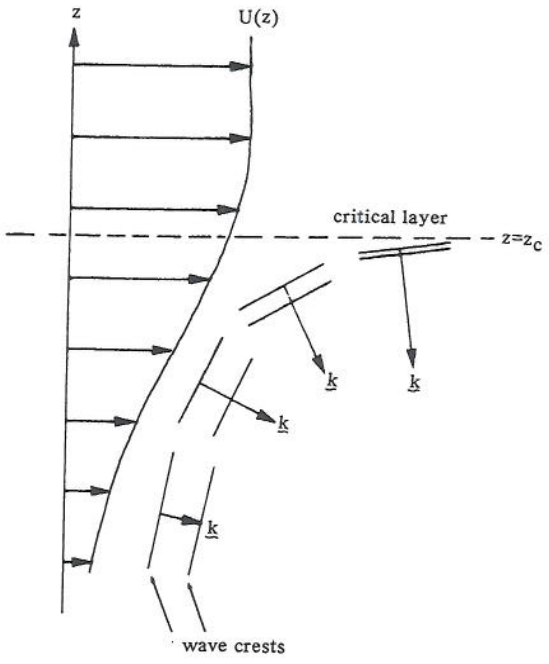

Fig. 5. The propagation of a wave packet upward toward a critical layer at $z=z_c$. The particle motions are parallel to the wave crests. Notice that the vertical wavelength becomes shorter as the wave packet approaches the critical level. (From LeBlond and Mysak, 1978, after Bretherton, 1966)

$$\frac{\partial u'}{\partial x} + \frac{\partial w'}{\partial z} = 0 \tag{39}$$

$$U\frac{\partial \theta'}{\partial x} + \frac{N^2\theta_o}{g}w' = \frac{\theta_o}{c_p T_o}q'. \tag{40}$$

The above physical system is identical to that investigated in Smith and Lin (1982) except that the perturbation potential temperature, instead of the perturbation density, is used as a dependent variable. These equations can be combined to give a single equation for the vertical velocity:

$$w'_{xx} + w'_{zz} + l^2(z)w' = \frac{g}{c_p T_o U^2}q', \tag{41}$$

where $l^2(z)=N^2/U^2$ is the Scorer parameter for a uniform basic flow, which has the form $l^2(z)=N^2/U^2-U_{zz}/U$ in general (Scorer, 1954). Similar to mountain wave theory (Smith, 1979), the above equation may be interpreted as a vorticity equation. Upon multiplying through by U, the $U(w'_{xx}+w'_{zz})$ term is the rate of change of perturbation vorticity following a fluid particle; N^2w'/U is the rate of perturbation vorticity generated by the buoyancy force; $-U_{zz}w'$ is the rate of perturbation vorticity generated by the vertical advection of the basic vorticity (U_z).

For a quasi-steady thermal forcing, such as the surface sensible heating over a heat island, the condensational heating associated with upslope orographic rain, or the evaporative cooling under a thunderstorm, we may prescribe the heating rate $q'(x, z)$. One simple way to obtain a mathematical solution is to assume a separable heating function,

$$q'(x,z) = Q_o f(x) g(z), \tag{42}$$

where $g(z)$ is normalized according to

$$\int_0^\infty g(z)\,dz = 1, \tag{43}$$

so that

$$\rho_o \int_0^\infty q'(x,z)\,dz = \rho_o Q_o f(x) \tag{44}$$

represents the total energy in a unit time added to a vertical column of the atmosphere. To avoid the net heating problem (Smith and Lin, 1982), we impose the constraint

$$\int_{-\infty}^{\infty} f(x)\,dx = 0 \tag{45}$$

at each level. To find the mathematical solution, we apply a Green's function method by assuming that the heating is concentrated at a height z_H,

$$q'(x,z)=Q_o f(x)\delta(z-z_H). \tag{46}$$

At the interface $z=z_H$, we require that the vertical velocity be continuous, i.e.

$$w'(z_H^+)-w'(z_H^-)=0. \tag{47}$$

Substituting (46) into (41) and integrating (41) from just below to just above $z=z_H$ gives the second interface condition:

$$w_z'(z_H^+)-w_z'(z_H^-)=\frac{g\,Q_o f(x)}{c_p T_o U^2}. \tag{48}$$

Away from the interface, Eq. (41) reduces to Scorer's equation:

$$w'_{xx}+w'_{zz}+l^2 w'=0. \tag{49}$$

The mathematical problem associated with Eqs. (47)–(49) with appropriate upper and lower boundary conditions is very similar to problems encountered in mountain wave theory, which was reviewed by Queney *et al.* (1960) and Smith (1979).

To simplify the mathematical problem and to avoid the complications induced by the wave reflection from the rigid, flat, lower boundary, we consider a sinusoidal heat source located at z_H=0 in an unbounded atmosphere:

$$q'(x,z)=Q_o\cos kx\,\delta(z). \tag{50}$$

We look for solutions of the form

$$w'(x,z)=w_1(z)\cos kx+w_2(z)\sin kx. \tag{51}$$

Thus, Scorer's equation, which governs solutions for w_i, becomes

$$w_{izz}+(l^2-k^2)w_i=0,\quad i=1,2. \tag{52}$$

To solve Eq. (52), we have to consider two cases: $k^2>l^2$ and $k^2<l^2$. For $k^2>l^2$, the solutions may be written as

$$w_i(x,z)=A_i(x)e^{-\sqrt{k^2-l^2}\,z}+B_i(x)e^{\sqrt{k^2-l^2}\,z},$$

$$\text{for } z>0$$

$$w_i(x,z)=C_i(x)e^{-\sqrt{k^2-l^2}\,z}+D_i(x)e^{\sqrt{k^2-l^2}\,z},$$

$$\text{for } z<0. \tag{53}$$

The B_i and C_i terms represent disturbances which grow in the vertical away from the heating level, and which should be eliminated because the energy source is located at z_H=0. This requires B_i=C_i=0. Applying the interface conditions (47) and (48) to (53), we obtain

$$w'(x,z)=\frac{-g\,Q_o}{2c_p T_o U^2\sqrt{k^2-l^2}}\cos kx\,e^{-\sqrt{k^2-l^2}\,|z|}$$

$$\text{for } k^2>l^2. \tag{54}$$

Thus, the above solution represents evanescent waves which satisfy boundedness conditions at $z=\pm\infty$. The condition $k^2>l^2$ corresponds to $2\pi/L>N/U$, which physically represents a relatively stronger wind with a weaker stability passing over a narrower heat source. The L denotes the horizontal wavelength of the heat source. Under this situation, it takes a longer time for an air parcel to undergo vertical oscillations with the Brunt-Vaisala frequency than to pass (be advected) over the heat source. In other words, the intrinsic frequency (Uk) is larger than the Brunt-Vaisala frequency. Thus, the wave energy cannot propagate away from the heat source in the vertical. Instead, it is trapped near the heating level and advected downstream. Therefore, there is no internal gravity wave generated. In the limit of $k^2\gg l^2$, the buoyancy force becomes extremely weak and can be ignored. In this limiting case, the disturbance will approach a potential flow.

For the case with $k^2<l^2$, the solution of (52) may be written as

$$w_i(z)=A_i\sin mz+B_i\cos mz,\quad i=1,2, \tag{55}$$

where $m^2=l^2-k^2$. Combining with Eq. (51), the above solution can be rewritten as

$$w'(x,z)=C\cos(kx+mz)+D\cos(kx-mz)$$
$$+E\sin(kx+mz)+F\sin(kx-mz)$$
$$\text{for } z>0. \tag{56a}$$

$$w'(x,z)=C'\cos(kx+mz)+D'\cos(kx-mz)$$
$$+E'\sin(kx+mz)+F'\sin(kx-mz)$$
$$\text{for } z<0. \tag{56b}$$

Terms with argument $kx+mz$ have an upstream phase

tilt while terms with argument $kx-mz$ have a downstream phase tilt. Mathematically, both of them satisfy the governing equation. However, they have different physical implications. To determine the proper solution, we must calculate the vertical energy flux. Let us consider the first term:

$$w'(x,z)=C\cos(kx+mz).$$

Using the continuity equation and the momentum equation, the vertical energy flux can be found to be

$$\int_0^L p'w'\,dx=\rho_o C^2 Um/k^2. \tag{57}$$

This represents an upward propagation of wave energy. Similarly, terms with argument $kx-mz$ represent a downward propagation of wave energy. Since the energy source is located at z=0, the upper and lower radiation conditions require $D=F=C'=E'=0$. Applying the interface conditions (47) and (48) to (56), we obtain

$$w'(x,z)=\frac{g\,Q_o}{2c_pT_oU^2\sqrt{l^2-k^2}}\sin(kx+\sqrt{l^2-k^2}\,|z|)$$

$$\text{for } k^2<l^2. \tag{58}$$

The above solution represents vertically propagating waves which satisfy radiation conditions at $z=\pm\infty$. The condition $k^2 < l^2$ corresponds physically to a relatively weaker wind with a stronger stability over a broader heat source. Under this situation, it takes a shorter time for an air parcel to experience vertical oscillation with the Brunt-Vaisala frequency than to pass (be advected) over the heat source. In other words, the intrinsic frequency (Uk) is smaller than the Brunt-Vaisala frequency. Thus, gravity waves can be generated, and the wave energy is able to propagate to positive or negative infinity (in an unbounded fluid) from the heat source. The flow response predicted by Eq. (58) becomes hydrostatic for $k^2 << l^2$. In this limit, the above equation reduces to

$$w'=\frac{g\,Q_o}{2c_pT_oU^2l}\sin(kx+l|z|). \tag{59}$$

Notice that the above solution repeats itself at a vertical wavelength of $2\pi U/N$. With a typical atmospheric situation of U=10 ms^{-1} and N=0.01 s^{-1}, the vertical wavelength of the forced wave is about 6.28 km.

We may define the vertical displacements as

$$w'=U\frac{\partial\eta}{\partial x}. \tag{60}$$

The vertical displacement for the hydrostatic case is shown in Fig. 6. Vertically propagating waves are evident above and below the heating level (z=0) with phase tilting upstream. Notice that the vertical displacement at the heating level is exactly out of phase with the heating rate. That is, the air parcel is displaced downward in the heating region, while it is displaced upward in the cooling region. Smith and Lin (1982) proposed a parcel argument to explain this phenomenon. This curious negative phase relationship between vertical displacement and heating will be explained later by considering the solution to the transient problem (Lin and Smith, 1986) and by using a group velocity argument (Bretherton, 1988). Proper upper and lower boundary conditions are necessary to obtain the correct solution. By using an incorrect radiation condition at infinity in a half-plane (semi-infinite fluid) in the heat island problem, Malkus and Stern (1953) obtained a positive relationship between the heating and the vertical displacement.

Similar to applications in mountain wave theory (Eliassen and Palm, 1960), the vertical transport of horizontal momentum can be calculated by

$$MF=\rho_o\int_0^L u'w'\,dx, \tag{61}$$

where L is the horizontal wavelength. From Eqs. (59) and (61), we obtain

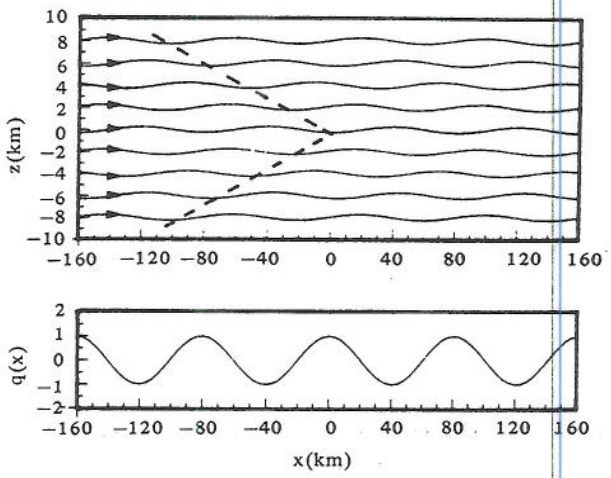

Fig. 6. The vertical displacement of an unbounded, hydrostatic, stratified airflow to periodic heating and cooling concentrated at the z=0 level, as given by Eqs. (54) and (52), with U=10 ms^{-1}, N=0.01 s^{-1}, k=40 km^{-1}, Q_o=1200 W m kg^{-1}, T_o=287 K. The heating rate function is shown at the bottom of the figure. Vertically propagating waves are evident from the upstream phase tilting above and below the heating level. (From Smith and Lin, 1982)

$$\frac{MF}{L}=\frac{-\rho_o}{2kl}\left(\frac{gQ_o}{2c_pT_oU^2}\right)^2\frac{z}{|z|}. \tag{62}$$

The transport of mechanical energy away from the layer of forcing is accompanied by a flux of horizontal momentum towards the layer.

To examine the effect of vertical momentum flux, we may consider the time-dependent nonlinear horizontal momentum equation

$$\frac{\partial u'}{\partial t}+U\frac{\partial u'}{\partial x}+\frac{1}{\rho_o}\frac{\partial p'}{\partial x}=-u'\frac{\partial u'}{\partial x}-w'\frac{\partial u'}{\partial z}. \tag{63}$$

Taking the horizontal integration over one wavelength yields

$$\frac{\partial \bar{u}}{\partial t}=-\frac{\partial}{\partial z}\overline{u'w'}, \tag{64}$$

where

$$\overline{(\ )}=\int_0^L(\ )\,dx. \tag{65}$$

Therefore, convergence of the vertical momentum flux, such as that in Eq. (62), tends to accelerate the flow. Notice that this acceleration is not explicitly accounted for in linear theory due to the neglecting of nonlinear terms. This acceleration may have relevance to the problems of wave-CISK (Raymond, 1986), heat islands, atmospheric tides, and orographic rain (Smith and Lin, 1982).

2. Isolated Heat Source and Topography

The above mathematical problem is illuminative in providing physical insight into the flow response. However, in applying the theory to atmospheric phenomena, such as the orographic rain problem (Smith and Lin, 1982), we need to consider a rigid irregular lower boundary and localized heat source.

A useful localized heating function may be chosen as

$$q'(x,z)=\frac{-2Q_ob^3x}{(x^2+b^2)^2}\delta(z-z_H). \tag{66}$$

The above heating function is shown in Fig. 7 as curve 1. This heating function can be used to simulate the condensational heating and evaporative cooling associated with a nonprecipitating orographic cloud. Again, we may apply the Green's function method to obtain the solution. The heating is concentrated at a certain

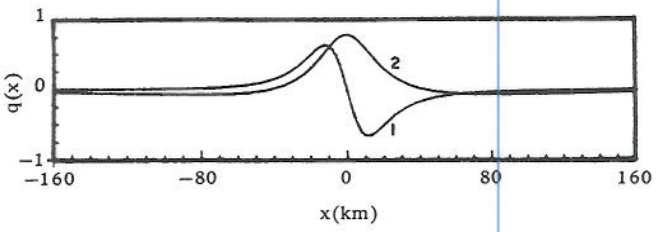

Fig. 7. The horizontal heating functions of Eq. (66) with b=20 km (curve 1) and Eq. (86) with b_1=20 km and b_2=100 km (curve 2). The balanced heating and cooling function (curve 1) is used to simulate the condensational heating and evaporative cooling associated with a nonprecipitating orographic cloud. Curve 2 is used to simulate the condensational heating associated with orographic rain, with isolated heating and widespread cooling. (From Smith and Lin, 1982)

level. Substituting the above equation into Eq. (41), we have

$$w'_{xx}+w'_{zz}+l^2w'=\frac{-2gQ_ob^3x}{c_pT_oU^2(x^2+b^2)^2}\delta(z-z_H). \tag{67}$$

Let $\tilde{w}(k,z)$ be the one-sided Fourier transform of $w'(x, z)$ in x, i.e.,

$$\tilde{w}(k,z)=\frac{1}{2\pi}\int_{-\infty}^{\infty}w'(x,z)e^{-ikx}dx \tag{68a}$$

$$w'(x,z)=2\,\mathrm{Re}\int_0^{\infty}\tilde{w}(k,z)e^{ikx}dk. \tag{68b}$$

Now taking the Fourier transform of Eq. (67), we obtain

$$\tilde{w}_{zz}+(l^2-k^2)\tilde{w}=\frac{igQ_ob^2k}{c_pT_oU^2}e^{-kb}\delta(z-z_H). \tag{69}$$

For $z\neq z_H$, (69) becomes Scorer's equation (Scorer, 1954):

$$\tilde{w}_{zz}+(l^2-k^2)\tilde{w}=0. \tag{70}$$

For a hydrostatic wave ($k^2<<l^2$), the solution may be written as

$$\tilde{w}(k,z)=Ae^{ilz}+Be^{-ilz}\quad \text{for } 0\le z<z_H \tag{71a}$$

$$\tilde{w}(k,z)=Ce^{ilz}+De^{-ilz}\quad \text{for } z_H\le z. \tag{71b}$$

At the ground, the flow is assumed to follow the terrain, thus

$$\frac{w}{u}=\frac{w'}{U+u'}=\frac{dh(x)}{dx}, \quad \text{at } z=h(x) \tag{72}$$

where $h(x)$ represents the terrain height. For small amplitude topography and induced disturbance, the above lower boundary condition may be written as

$$w'=U\frac{dh(x)}{dx}, \quad \text{at } z=0. \tag{73}$$

For mathematical simplicity, we consider a bell-shaped function to represent the topography which is often used in mountain wave theory (e.g., Smith, 1979):

$$h(x)=\frac{h_o a^2}{(x^2+a^2)}. \tag{74}$$

Substituting (74) into (73) and taking the Fourier transform, we obtain

$$\tilde{w}(k,0)=ikUh_o a e^{-ka}. \tag{75}$$

Applying the lower boundary condition (75) to (71a) gives

$$A+B=ikUh_o a e^{-ka}. \tag{76}$$

The upper radiation boundary condition should allow the wave energy to propagate upward (Eliassen and Palm, 1960; Bretherton, 1969). This can be determined by computing the vertical energy flux similar to Eq. (57), which requires D=0. With (76) and this upper boundary condition, (71) becomes

$$\tilde{w}(k,z)=2iA\sin lz+ikUh_o a e^{-ka}e^{-ilz}, \quad \text{for } 0\le z<z_H \tag{77a}$$

$$\tilde{w}(k,z)=Ce^{ilz}, \quad \text{for } z\ge z_H. \tag{77b}$$

In the above solution, we allow the thermally forced wave to propagate downward toward the surface below the heating level z_H. Coefficients A and C in (77) can be determined by the two interface conditions (47) and (48). In the Fourier space, they have the following forms:

$$\tilde{w}(z_H^+)-\tilde{w}(z_H^-)=0, \tag{78a}$$

$$\tilde{w}_z(z_H^+)-\tilde{w}_z(z_H^-)=\frac{igQ_o b^2 k e^{-bk}}{c_p T_o U^2}. \tag{78b}$$

Applying the above equation to (77) and taking the inverse Fourier transform leads to

$$w'(x,z)=2\,\mathrm{Re}\{\int_0^\infty [iUh_o ake^{-ka}e^{ilz} - \frac{igQ_o b^2 k e^{-kb}e^{ilz_H}\sin lz}{c_p T_o U^2 l}]e^{ikx}dk\}$$

$$\text{for } 0\le z<z_H$$

$$w'(x,z)=2\,\mathrm{Re}\{\int_0^\infty [iUh_o ake^{-ka}e^{ilz} - \frac{igQ_o b^2 k e^{-kb}e^{ilz}\sin lz_H}{c_p T_o U^2 l}]e^{ikx}dk\}$$

$$\text{for } z\ge z_H. \tag{79}$$

Using the relationship (60), the vertical displacement can be obtained:

$$\eta(x,z)=\eta_m(x,z)-\frac{gQ_o b^2\sin lz(b\cos lz_H - x\sin lz_H)}{c_p T_o U^3 l(x^2+b^2)}$$

$$\text{for } 0\le z<z_H \tag{80a}$$

$$\eta(x,z)=\eta_m(x,z)-\frac{gQ_o b^2\sin lz_H(b\cos lz - x\sin lz)}{c_p T_o U^3 l(x^2+b^2)}$$

$$\text{for } z_H\le z, \tag{80b}$$

where

$$\eta_m(x,z)=\frac{h_o a(a\cos lz - x\sin lz)}{x^2+a^2}. \tag{80c}$$

Notice that the above solution is a superposition of the hydrostatic mountain wave (η_m) and the thermally forced gravity wave.

The pressure perturbation at the surface can be computed from (80) using either Bernoulli's equation (substituting Eqs. (39) and (60) into Eq. (37)),

$$p'(x,0)=-\rho_o U u'(x,0)=\rho_o U^2\frac{\partial\eta}{\partial z}\Big|_{z=0} \tag{81}$$

or the hydrostatic equation (with Eq. (40)),

$$p'(x,0)=\frac{g\rho_o}{\theta_o}\int_0^\infty \theta' dz$$

$$=-\rho_o N^2 \int_0^\infty \eta(x,z)\,dz-\frac{g\rho_o Q_o}{c_p T_o U}\int_{-\infty}^{x} f(x)\,dx. \quad \textbf{(82)}$$

Either approach gives

$$p'(x,0)=-\rho_o N U h_o \frac{ax}{x^2+a^2}-\frac{\rho_o g Q_o b^2}{c_p T_o U^2}$$

$$\cdot\{\frac{(b\cos l z_H - x\sin l z_H)}{(x^2+b^2)}\}. \quad \textbf{(83)}$$

The first terms (η_m) of Eqs. (80) and (83) represent the vertical displacement and surface pressure perturbation produced by the mountain wave, which have been found by Queney (1947) and studied extensively in the literature (e.g., see Smith, 1979 for a review). The second terms of Eqs. (80) and (83) represent the vertical displacement and surface pressure disturbance produced by the thermally induced gravity wave, which satisfy the rigid lower boundary condition $w'=0$ at $z=0$; thus, the downgoing wave produced by the elevated heating is totally reflected. The vertical momentum flux is zero between the heating level and the surface, due to the flux cancellation of the up and downgoing waves. This gives no vertical phase tilt of the disturbance. The flow response is sensitive to the heating level since the upgoing and downgoing waves may cancel each other. If the heating is added very near the surface, $lz_H << l$, the disturbance is extremely small and may be neglected. From Eq. (80), cancellation of the direct upgoing wave and the reflected upgoing wave above z_H can also occur at

$$l z_H = 0, \pi, 2\pi, ..., n\pi.$$

This effect is less evident if the heating is spread over a layer of finite depth.

For a heat source distributed uniformly in a layer of $z = z_H - d$ to $z_H + d$, the solution can be obtained by superposition of heating terms of (80a and b) (the last terms). In order to keep the same heating rate, the amplitude of this vertically distributed heating should be reduced to $Q_o/2d$. If we write (80a) and (80b) as $\eta = \eta_m + \eta_H^-$ and $\eta = \eta_m + \eta_H^+$, respectively, then the superposition of heating terms leads to

$$\eta(x,z)=\eta_m(x,z)+\int_{z_H-d}^{z_H+d}\eta_H^-(x,z,z')\,dz'$$

$$\text{for } 0 \le z < z_H - d, \quad \textbf{(84a)}$$

$$\eta(x,z)=\eta_m(x,z)+\int_{z_H-d}^{z}\eta_H^+(x,z,z')\,dz'$$

$$+\int_{z}^{z_H+d}\eta_H^-(x,z,z')\,dz'$$

$$\text{for } z_H - d \le z < z_H + d, \quad \textbf{(84b)}$$

$$\eta(x,z)=\eta_m(x,z)+\int_{z_H-d}^{z_H+d}\eta_H^+(x,z,z')\,dz'$$

$$\text{for } z_H + d \le z, \quad \textbf{(84c)}$$

where z' represents z_H in (80) and acts as an integral variable in the above equation. The final solution can be obtained:

$$\eta(x,z)=\eta_m(x,z)-\frac{g Q_o b^2 \sin l z}{c_p T_o U^3 l^2 (x^2+b^2)}$$

$$\cdot[b\{\sin l(z_H+d)-\sin l(z_H-d)\}$$

$$+x\{\cos l(z_H+d)-\cos l(z_H-d)\}]$$

$$\text{for } 0 \le z < z_H - d \quad \textbf{(85a)}$$

$$\eta(x,z)=\eta_m(x,z)+\frac{g Q_o b^2}{c_p T_o U^3 l^2 (x^2+b^2)}\{(b\cos l z$$

$$-x\sin l z)\{\cos l z-\cos l(z_H-d)\}$$

$$-\sin l z[b\{\sin l(z_H+d)-\sin l z\}$$

$$+x\{\cos l(z_H+d)-\cos l z\}]\}$$

$$\text{for } z_H - d \le z < z_H + d \quad \textbf{(85b)}$$

$$\eta(x,z)=\eta_m(x,z)+\frac{g Q_o b^2}{c_p T_o U^3 l^2 (x^2+b^2)}(b\cos l z$$

$$-x\sin l z)\{\cos l(z_H+d)-\cos l(z_H-d)\}$$

$$\text{for } z_H + d \le z. \quad \textbf{(85c)}$$

Another useful heating function is

$$q'(x,z)=Q_o\left(\frac{b_1^2}{x^2+b_1^2}-\frac{b_1 b_2}{x^2+b_2^2}\right)\delta(z-z_H), \quad \textbf{(86)}$$

where b_1 and b_2 are the half-width of the isolated heating and the widespread compensated cooling, respectively. The widespread cooling is used to avoid the net heating problem (Smith and Lin, 1982). This problem will be discussed in Section IV. The above function may be used to simulate the condensational heating associated with a precipitating orographic cloud. Applying the method used above, the following solutions may be derived:

$$\eta(x,z)=\eta_m(x,z)-\frac{g\,Q_o\,b_1\sin l\,z}{c_p\,T_o\,U^3\,l}\{(\cos l\,z_H)(\tan^{-1}\frac{x}{b_1}-\tan^{-1}\frac{x}{b_2})+\frac{1}{2}(\sin l\,z_H)\ln(\frac{x^2+b_2^2}{x^2+b_1^2})\}$$

for $0 \le z < z_H$ **(87a)**

$$\eta(x,z)=\eta_m(x,z)-\frac{g\,Q_o\,b_1\sin l\,z_H}{c_p\,T_o\,U^3\,l}\{(\cos l\,z)(\tan^{-1}\frac{x}{b_1}-\tan^{-1}\frac{x}{b_2})+\frac{1}{2}(\sin l\,z)\ln(\frac{x^2+b_2^2}{x^2+b_1^2})\}$$

for $z_H \le z$. **(87b)**

The perturbation surface pressure associated with (87) is

$$p'(x,0)=-\rho_o N U h_o\frac{a\,x}{x^2+a^2}-\frac{\rho_o g\,Q_o\,b_1}{c_p\,T_o\,U}\cdot\{(\cos l\,z_H)(\tan^{-1}\frac{x}{b_1}-\tan^{-1}\frac{x}{b_2})+\frac{1}{2}(\cos l\,z_H)\ln(\frac{x^2+b_2^2}{x^2+b_1^2})\}. \quad \textbf{(88)}$$

If this isolated heat source is distributed uniformly in a layer from $z = z_H - d$ to $z_H + d$, the method of superposition discussed above may be used to obtain the result:

$$\eta(x,z)=\eta_m(x,z)-\frac{g\,Q_o\,b_1\sin l\,z}{c_p\,T_o\,U^3\,l^2}\{(\tan^{-1}\frac{x}{b_1}-\tan^{-1}\frac{x}{b_2})[\sin l(z_H+d)-\sin l(z_H-d)]-\frac{1}{2}\ln(\frac{x^2+b_2^2}{x^2+b_1^2})[\cos l(z_H+d)-\cos l(z_H-d)]\}$$

for $0 \le z < z_H$ **(89a)**

$$\eta(x,z)=\eta_m(x,z)+\frac{g\,Q_o\,b_1}{c_p\,T_o\,U^3\,l^2}\{(\cos l\,z)(\tan^{-1}\frac{x}{b_1}-\tan^{-1}\frac{x}{b_2})+\frac{1}{2}(\sin l\,z)\ln(\frac{x^2+b_2^2}{x^2+b_1^2})[\cos l\,z-\cos l(z_H-d)]\}-\frac{g\,Q_o\,b_1\sin l\,z}{c_p\,T_o\,U^3\,l^2}\{(\tan^{-1}\frac{x}{b_1}-\tan^{-1}\frac{x}{b_2})[\sin l(z_H+d)-\sin l\,z]-\frac{1}{2}\ln(\frac{x^2+b_2^2}{x^2+b_1^2})[\cos l(z_H+d)-\cos l\,z]\}$$

for $z_H - d \le z < z_H + d$ **(89b)**

$$\eta(x,z)=\eta_m(x,z)+\frac{g\,Q_o\,b_1}{c_p\,T_o\,U^3\,l^2}\{(\cos l\,z)(\tan^{-1}\frac{x}{b_1}-\tan^{-1}\frac{x}{b_2})+\frac{1}{2}(\sin l\,z)\ln(\frac{x^2+b_2^2}{x^2+b_1^2})\}\cdot[\cos l(z_H+d)-\cos l(z_H-d)]$$

for $z_H + d \le z$. **(89c)**

The hydrostatic response of a balanced heating and cooling (Eq. (66)) added at $z_H = \pi/2l$ E 1.57 km is given in Fig. 8. The solution is given by the second terms of (80) with Q_o=1107 Wmkg^{-1}, b=20 km, U = 10 ms^{-1}, and N = 0.01 s^{-1}. The upstream phase tilt of the thermally forced gravity waves is evident above the heating level. Notice that a downward displacement is produced near the heating region and upward displacement near the cooling region. The result of Malkus and Stern (1953) would be similar to the present one if they used the correct upper radiation condition. This relationship will be explained in the next section. The vertical displacement at the heating level is repeated every 6.28 km ($2\pi/l$). The surface perturbation pressure is shown in the lower panel of Fig. 8. The hydrostatic equation indicates that the surface pressure is an integral measure of the temperature or density anomaly aloft. Equation (82) or the thermodynamic equation implies that the temperature anomaly may be caused directly by the heating and indirectly by the thermally-induced vertical motion. According to Bernoulli's equation, the wind speed is increased when the streamlines are closer together. One example of the response of a hydrostatic airflow over this isolated heating and compensated cooling (Eq. (86)) is shown in Fig. 9. The heating is added at $z_H = \pi/2l$. The solution is given by Eq. (87) with η_m ignored and Q_o=900 Wm kg^{-1}, b_1=20 km, b_2=100 km, U=10 ms^{-1}, and N=0.01 s^{-1}. The response is similar to the previous case. The relationship between the thermal response in a system with and without a basic flow was discussed by Thorpe *et al.* (1980). The large Froude number results in that paper are in qualitative agreement with the present results. Hsu (1987a, b) found a similar result for a mesoscale flow over a finite surface heating. The heating in that

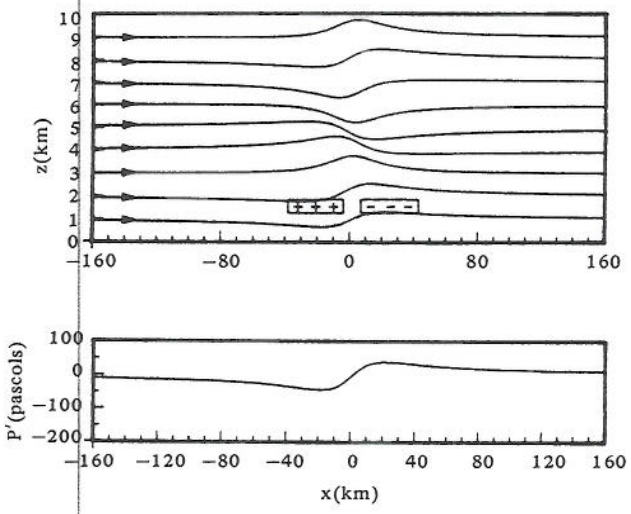

Fig. 8. The vertical displacement of a hydrostatic airflow to balanced heating and cooling (Eq. (66)) concentrated at z_H=1.57 km in an half plane. Regions with large heating and cooling are marked +++ and − − −, respectively. This flow is given by the second terms of Eq. (80) with Q_o=1107 W m kg^{-1}, b=20 km, U=10 ms^{-1}, and N=0.01 s^{-1}. Vertically propagating waves are present above the heating level. The surface pressure disturbance (in Pa) is shown in the lower panel. (From Smith and Lin, 1982)

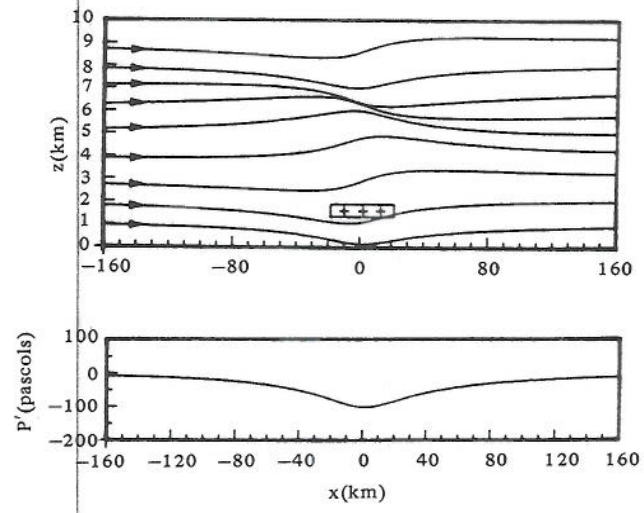

Fig. 9. Same as Fig. 8 except for the isolated heating-widespread cooling function (86). The solution is given by the second terms of Eq. (87) with Q_o=900 W m kg^{-1}, b_1=20 km, b_2=100 km, U=10 ms^{-1}, and N=0.01 s^{-1}. The perturbation surface pressure is shown in the lower panel, which is negative directly below the region of heating. (From Smith and Lin, 1982)

paper is added into the system through conduction by prescribing the perturbation surface potential temperature.

3. Applications

The theory developed in Section III.2 has been applied to the problem of orographic rain by Smith and Lin (1982, 1983). Based on the formation mechanisms, the orographic rain may be classified as follows:

(1) Upslope orographic rain in a stable atmosphere (Sarker, 1967).
(2) Orographic rain in a conditionally unstable atmosphere (Davies and Schar, 1986).
  (a) upslope rain, instability released by forced orographic ascent.
    (i) shallow convection embedded within frontal clouds in midlatitude (Browning *et al.*, 1974; Browning, 1980; Hobbs *et al.*, 1975; Marwitz, 1980).
    (ii) closely packed deep convection in tropics (Smith and Lin, 1983).
  (b) lee convective rain, instability triggered by slope heating (Henz, 1972).
(3) Orographic rain over small hills by seeder cloud-feeder cloud mechanism (Bergeron, 1968; Browning, 1980).
(4) Existing baroclinicity which, through the action of orographic blocking and differential advection, can lead to an unstable air column (Smith, 1982).

For a quasi-steady nonprecipitating orographic cloud, the condensational heating and evaporative cooling may be represented by the balanced heating and cooling (Eq. (66)). An example of a hydrostatic airflow over a bell-shaped mountain with and without diabatic heating is given in Fig. 10. The disturbance induced by combined mechanical and thermal forcing is weaker than the adiabatic flow (Fig. 10a). The vertical displacement near the heating region is consistent with previous results. That is, heating (cooling) produces downward (upward) displacement. The relative magnitude of the response can be found from the ratio of the two coefficients in Eq. (80),

$$\frac{g\,Q_o\,b}{c_p\,T_o\,U^2\,N\,h_o},$$

where Q_o and b are roughly related to the intensity and the horizontal scale of the observed rainfall at the surface. Figure 11 shows two examples of hydrostatic responses in a stratified airflow to isolated thermal and orographic forcing. The solution is given by Eq. (87) with x in the second terms replaced by $x+c$, where c is the upstream distance between the heating center and the mountain top. Notice the significant difference in the flow patterns due to the different upstream dis-

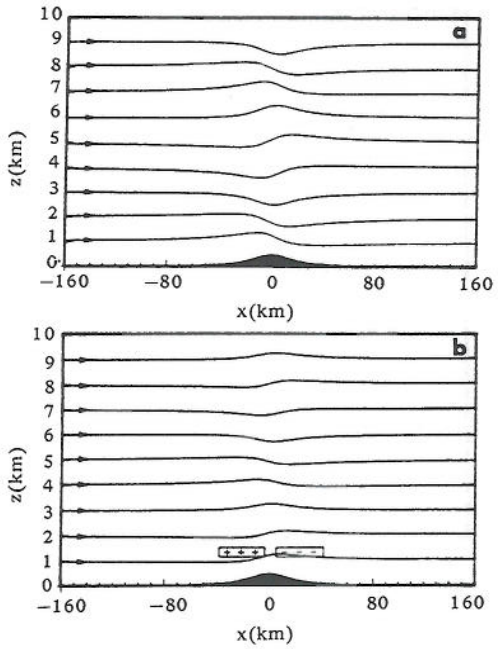

Fig. 10. (a) The vertical displacement of a hydrostatic adiabatic flow over a bell-shaped mountain. The solution was first derived by Queney (1947) and is given by Eq. (80c) with h_o=500 m, a=20 km, U=10 ms^{-1}, and N=0.01 s^{-1}. (b) Hydrostatic flow over a combined thermal and orographic forcing. The prescribed diabatic heating represents a nonprecipitating orographic cloud. The solution is given by Eq. (80a and b) with Q_o=1107 W m kg^{-1}, b=20 km, U=10 ms^{-1}, and N=0.01 s^{-1}. The induced disturbance is weaker than the adiabatic mountain wave (a). (From Smith and Lin, 1982)

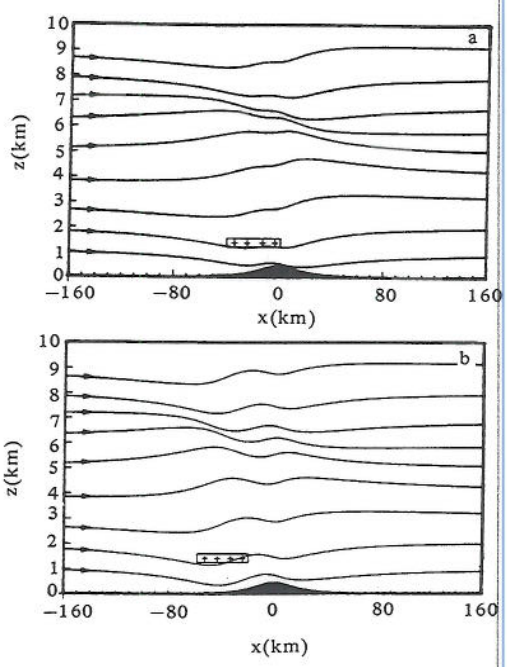

Fig. 11. The vertical displacement of a hydrostatic flow over combined thermal and orographic forcing. The diabatic heating represents an upslope precipitating orographic rain. The solution is given by Eq. (87) with x replaced by x+c and Q_o=900 W m kg^{-1}, b_1=20 km, b_2=100 km, U=10 ms^{-1}, and N=0.01 s^{-1}. The upstream displacement of heating of c=20 km is shown in (a) and c=40 km in (b). (From Smith and Lin, 1982)

placements of the thermal forcing.

The significance of the combined thermal and orographic forcing can be seen from the vertical transport of horizontal momentum. The momentum flux corresponding to Eq. (87) with x replaced by x+c is

$$MF=-\frac{\pi}{4}\rho_o h_o^2 N U-\left(\frac{\pi a g \rho_o h_o Q_o b_1}{c_p T_o U}\right)$$

$$\cdot\left[\frac{(a+b_1)\cos l z_H - c\sin l z_H}{(a+b_1)^2+c^2}\right.$$

$$\left.-\frac{(a+b_2)\cos l z_H - c\sin l z_H}{(a+b_2)^2+c^2}\right] \quad \text{for } 0 \le z < z_H \qquad \textbf{(90a)}$$

$$MF=-\frac{\pi}{4}\rho_o h_o^2 N U-\frac{\pi\rho_o}{l}\left(\frac{g Q_o b_1 \sin l z_H}{c_p T_o U^2}\right)^2$$

$$\cdot\ln\left[\frac{(b_1+b_2)^2}{4 b_1 b_2}\right]+\left(\frac{\pi a g \rho_o h_o Q_o b_1 \sin l z_H}{c_p T_o U}\right)$$

$$\cdot\left[\frac{2c}{(a+b_1)^2+c^2}-\frac{2c}{(a+b_2)^2+c^2}\right]. \quad \text{for } z_H \le z \qquad \textbf{(90b)}$$

The first terms in the above equation result from the vertically propagating mountain waves, which are negatively proportional to the vertical energy flux, which is constant with height for an adiabatic flow with no critical level and diabatic heating (Eliassen and Palm, 1960). Note that besides the pure h^2 and Q_o^2 terms there are cross terms proportional to h_oQ_o. The existence of this important contribution to the momentum flux below the heating level (Eq. (90a)) can be explained as arising physically from the thermally generated pressure disturbance at the surface, acting on the topography. It could, therefore, be computed directly from the perturbation surface pressure (Eq. (88)) together with (74). If a large amount of heating occurs over the windward slope of a mountain, the pressure at the surface could be lowered sufficiently to cause a reversal of the expected downstream drag. The vertical profiles of momentum flux corresponding to the adiabatic mountain wave (Fig. 10a) and the thermally and orographically forced wave (Fig. 11a) are shown in Fig. 12. In Eq. (90), the cross terms of the momentum flux depend

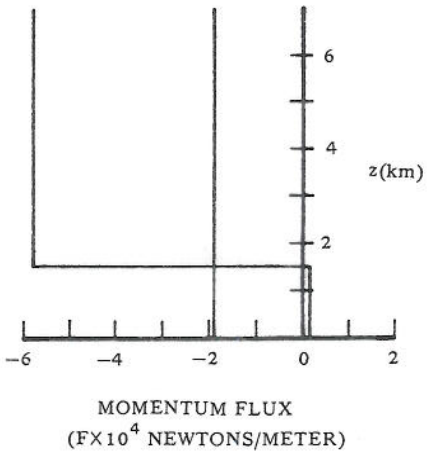

Fig. 12. The vertical profile of momentum flux for the cases shown in Figs. 10a and 11a as given by Eq. (90). In an adiabatic flow, the flux is constant with height. In the presence of thermal forcing, the mountain drag is reversed, and the momentum flux is strongly convergent at the heating level. (From Smith and Lin, 1982)

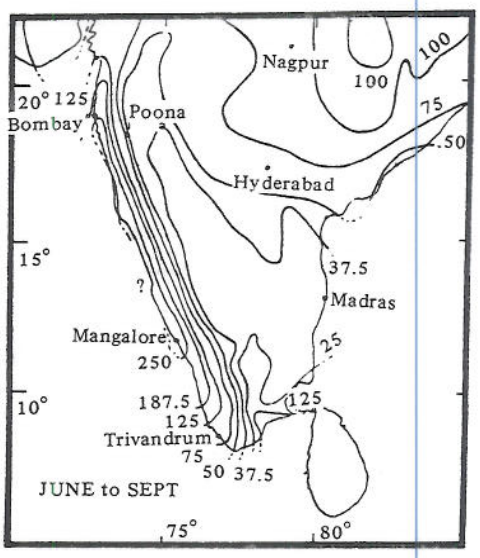

Fig. 13. The areal distribution of rainfall over India during the summer monsoon months of June to September (from Smith and Lin, 1983, after Ramakrishan and Rao, 1958). The rainfall is concentrated just upstream of the Western Ghats.

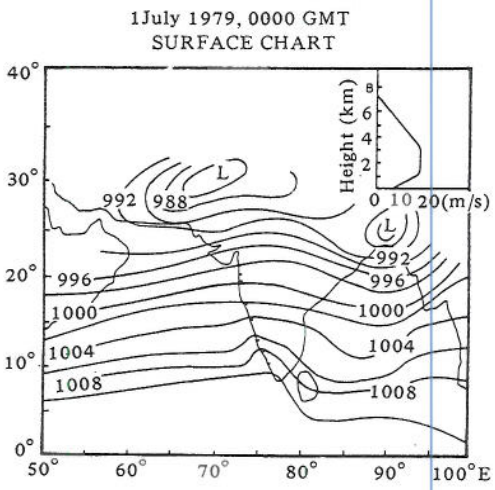

Fig. 14. A typical surface chart for the Indian Ocean during the summer monsoon. This particular chart is for 1 July 1979 at 0000 GMT. The horizontal wind perpendicular to the coast is shown at the upper right corner. (From Smith and Lin, 1983)

on the relative horizontal position of the heating and the mountain, i.e., c. As mentioned earlier, the pure thermally induced flux (Q_o^2) term must vanish below the heating level because of wave reflection from the surface.

A good example of the local enhancement of precipitation by orography is the large annual rainfall recorded along the Malabar Coast and on the windward slopes of the Western Ghats in India (Fig. 13). This rainfall occurs almost entirely during the 3-4 month summer period when the coast lies in the path of the west-southwest monsoon current crossing the Arabian Sea (Fig. 14). The low-level wind has a speed of about 15 ms^{-1} (at 850 mb), and a direction more or less perpendicular to the coast. In the upper troposphere, the wind is reversed, blowing from the east as part of the subtropical easterly. Figure 15 shows a hydrostatic flow with combined thermal and orographic forcing (Smith and Lin, 1983). The heating is producing a disturbance which is at least as large as that of the mountain. As mentioned earlier (Eq. (80)), the thermally-induced disturbance is moderately sensitive to the choice of lz_H. For the present choice of z_H=3 km, there is a region of strong low-level convergence and ascent which may be able to trigger cumulus growth. This choice is reasonable as waves generated in the upper troposphere would be absorbed by the critical level in midtroposphere (Fig. 14). Figure 15 also indicates that there is a wide pressure trough produced by the heating, which is absent in the adiabatic case. The pressure trough may be related to the offshore trough often observed during the rainy spell of the monsoon period.

Using the data from WMO/ICSU Summer Monsoon Experiment and a two-dimensional nonlinear model, Grossman and Durran (1984) have shown that the Western Ghats produce a deceleration and convergence of the southwest monsoon winds, triggering deep convection over the Arabian Sea. The results seem consistent with results of Smith and Lin (1983). However, as commented on by Smith (1985), the effect of latent heating has been omitted in that study. Using a two-

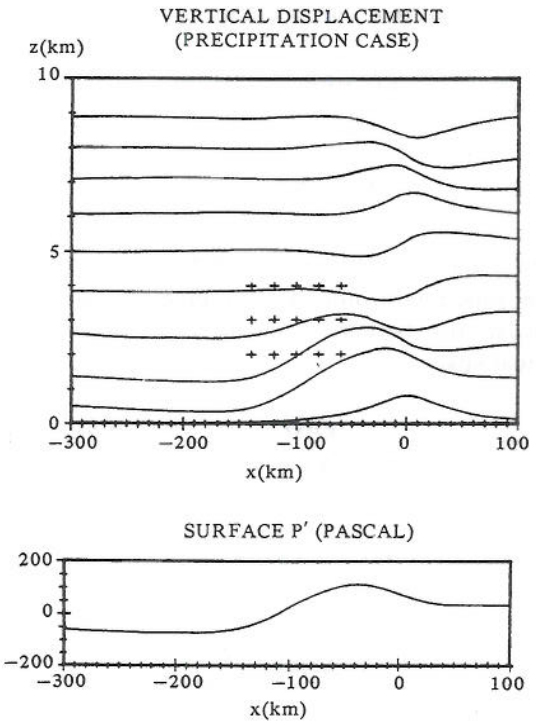

Fig. 15. The vertical displacement of a hydrostatic flow with thermal and orographic forcing. Region of the isolated heating is denoted by "+++". The solution is given by Eq. (89) with Q_o=1200 Wmkg^{-1}, b_1=40 km, b_2=200 km, a=40 km, h_o=800 m, z_H=3 km, d=1.5 km, U=10 ms^{-1}, and N=0.01 s^{-1}. The heating center is displaced upstream by 100 km (c). The surface perturbation pressure is drawn at the bottom. Note that there is a wide pressure trough produced by the heating. (From Smith and Lin, 1983)

dimensional compressible moist cloud model to simulate flow over the Western Ghats, Ogura and Yoshizaki (1988) find that in order to account for the observed features of rainfall over the Arabian Sea and the Ghat Mountains during the summer monsoon season, the strongly sheared environment and fluxes of latent and sensible heat from the ocean are essential. It appears that a theory which includes these factors can be constructed, similar to that of Lin (1987), and compared with the numerical results of Ogura and Yoshizaki. The combined effect of thermal and orographic forcing has also been studied by Davies and Schar (1986). In their theory, they incorporated a CISK-like representation for non-precipitating convective cloud in a linear, steady, hydrostatic flow over a mountain ridge. They found that the combined effect of the two forcing processes can be significantly different from that of orography acting alone. In particular, in certain situations an enhanced (resonant) response can occur with strong winds on the lee slope and a concomitant large surface pressure drag. Their results help to clarify the disparate results obtained in earlier studies, and, unlike those studies, suggest that diabatic effects might on occasions have a major role in inducing strong surface lee-side winds.

Similar theories have also been developed and applied to the mesoscale lake-effects on the generation of snowstorms in the vicinity of Michigan Lake (Hsu, 1987a, b) and the steady state response of the atmosphere to prescribed temperature perturbations corresponding to melting snow (Lin, C.A. *et al.*, 1988a, b; Robichaud and Lin, C.A., 1989).

IV. Transient Flow over a Meso-γ Scale Heat Source

Mesoscale problems of thermal or mechanical forcing cannot be fully understood using a steady state model. The importance of solving a time-dependent problem has been demonstrated in the studies of mountain waves (e.g., Hoiland, 1951; Palm, 1953; Queney, 1954), which provided insight into how a forced perturbation is established when the wind becomes practically steady over mountainous terrain. The transient heat island problem has been treated by Smith (1957), but without a full discussion of the energetics and the problematic approach to steady state. The internal gravity waves generated by local prescribed heating have been investigated by Blumen and Hendl (1969) with application to Joule heating in the ionsphere. The mathematical problem of wave generation by local thermal sources also arises in the study of large explosions (e.g., Pekeris, 1948; Scorer, 1950; Hunt *et al.*, 1960; Weston, 1962). These studies, however, are primarily concerned with the far field radiation of acoustic-gravity waves. In this section, we will review the transient response of a flow to a meso-γ scale heat source investigated by Lin and Smith (1986).

1. Flow Response to a Pulse Heating

Consider a two-dimensional, inviscid, nonrotating, hydrostatic, Boussinesq flow. The governing equation can be reduced from Eq. (15) or extended from Eq. (41) to be

$$(\frac{\partial}{\partial t}+U\frac{\partial}{\partial x})^2 w'_{zz}+N^2 w'_{xx}=\frac{g}{c_p T_o} q'_{xx}. \qquad (91)$$

To solve the above equation, we again apply the Green's function method in the vertical direction. Taking the Fourier transform in x ($x \rightarrow k$) and Laplace transform in t ($t \rightarrow s$) of the above equation, we have

$$\hat{w}_{zz}+\lambda^2\hat{w}=\frac{g\lambda^2}{c_pT_oN^2}\hat{q}, \tag{92}$$

where

$$\lambda\equiv\frac{iNk}{s+iUk}, \text{ and } \mathrm{Re}(s)>0.$$

Assume the heating is released in a very short time period as a pulse at a single level, z=0, in an unbounded fluid:

$$q'(t,x,z)=Q_o\left(\frac{b^2}{x^2+b^2}\right)\delta(z)\delta(t). \tag{93}$$

Taking the Fourier and Laplace transforms of the above equation and substituting into Eq. (92) gives

$$\hat{w}_{zz}+\lambda^2\hat{w}=\frac{gQ_obk^2e^{-bk}}{c_pT_oN^2}\delta(z). \tag{94}$$

Similar to the steady state problem, the interface condition can be obtained by assuming the continuity of the vertical velocity at the interface (z=0) and integrating the above equation across it. That is,

$$\hat{w}(0^+)-\hat{w}(0^-)=0, \tag{95}$$

$$\hat{w}_z(0^+)-\hat{w}_z(0^-)=\frac{gQ_obk^2e^{-bk}}{c_pT_oN^2}. \tag{96}$$

An appropriate set of upper and lower boundary conditions for an unbounded fluid are the Sommerfeld radiation conditions, i.e.

$$\hat{w}\sim e^{i\lambda|z|} \quad \text{as } |z|\to\infty. \tag{97}$$

Thus, the solution of Eq. (94) can be obtained:

$$\hat{w}(s,k,z)=\frac{-igQ_ob}{2c_pT_oN^2}\lambda e^{-bk}e^{i\lambda|z|}. \tag{98}$$

The above solution decays at infinity because Re(s)>0. The vertical displacement, η, defined by

$$w'=\frac{D\eta}{Dt}=\frac{\partial\eta}{\partial t}+U\frac{\partial\eta}{\partial x}, \tag{99}$$

may be written as

$$\hat{\eta}(s,k,z)=\frac{gQ_obke^{-bk}}{2c_pT_oN(s+iUk)^2}\exp\left(-\frac{Nk|z|}{s+iUk}\right). \tag{100}$$

The inverse Laplace transform of the above equation can be carried out to obtain

$$\tilde{\eta}(t,k,z)=\frac{gQ_obke^{-bk}}{2c_pT_o}\left(\frac{t}{Nk|z|}\right)^{1/2}e^{-iUkt}\cdot J_1(2\sqrt{Nk|z|t}), \tag{101}$$

where $\tilde{\eta}$ denotes the Fourier transform of η and J_1 the Bessel function of order 1. The inverse Fourier transform can also be carried out to yield the solution in physical space

$$\eta(t,x,z)=\frac{gbQ_ot}{2c_pT_oN(X^2+b^2)^2}\exp\left(-\frac{Nbt|z|}{X^2+b^2}\right)\cdot\left[(b^2-X^2)\cos\left(\frac{NtX|z|}{X^2+b^2}\right)+2bX\sin\left(\frac{NtX|z|}{X^2+b^2}\right)\right], \tag{102}$$

where $X = x - Ut$ is the horizontal coordinate in the reference frame moving with the basic wind. In the moving frame, the above equation is just the response of the fluid to a pulse heating in a quiescient stratified fluid.

The solution for a more realistic heating function in the vertical can be obtained by use of the Green's function method. The rigid lower boundary can also be incorporated by applying the method of images. The vertical displacement for a pulse heating distributed uniformly in a layer from $z_o - d$ to $z_o + d$ in a half plane can be written as

$$\begin{aligned}\eta(t,x,z)=\frac{A}{(X^2+b^2)}\{&2b[S(z_o-d)-S(z_o+d)]\\&+\mathrm{sgn}(z-z_o-d)e^{-bB|z-z_o-d|}\\&\cdot[X\sin(BX|z-z_o-d|)\\&+b\cos(BX|z-z_o-d|)]-\mathrm{sgn}(z-z_o+d)\\&\cdot e^{-bB|z-z_o+d|}[X\sin(BX|z-z_o+d|)\\&+b\cos(BX|z-z_o+d|)]+e^{-bB(z+z_o+d)}\\&\cdot(X\sin[BX(z+z_o+d)]\\&+b\cos[BX(z+z_o+d)])-e^{-bB(z+z_o-d)}\\&\cdot(X\sin[BX(z+z_o-d)]\\&+b\cos[BX(z+z_o-d)])\},\end{aligned} \tag{103}$$

where

$$A=\frac{g\,b\,Q_o}{2\,c_p\,T_o\,N^2},\quad B=\frac{N\,t}{X^2+b^2}.$$

The symbol S and sgn denote the step function and the sign function, respectively. The above equation is an extension of the result of Raymond (1983) as it allows a heating distribution of finite width and height and includes the advection effect of a constant basic wind. The last two terms, which include $z+z_o+d$ and $z+z_o-d$, are the effects of wave reflection from the lower boundary. If these two terms are excluded, the response of the unbounded fluid to a heat source distributed in a layer of finite depth has the form of a region of mostly upward displacements drifting with the basic wind.

The vertical displacement at the center of the heating layer, z=0, in the unbounded fluid can be written as

$$\hat{\eta}=\left(\frac{1}{\hat{x}^2+1}\right)\left\{1-\exp\left(\frac{-\hat{t}}{\hat{x}^2+1}\right)\left[\hat{x}\sin\left(\frac{\hat{t}\,\hat{x}}{\hat{x}^2+1}\right)+\cos\left(\frac{\hat{t}\,\hat{x}}{\hat{x}^2+1}\right)\right]\right\}, \tag{104}$$

where the nondimensional variables are defined as

$$\hat{x}=\frac{x-U\,t}{b},\ \hat{t}=\frac{N\,d\,t}{b},\ \hat{\eta}=\frac{c_p\,T_o\,N^2}{g\,Q_o}\,\eta(x,0,t). \tag{105}$$

We are interested in two regions: (a) the region of the drifting heated air and (b) the region of the initial heating. Figure 16a shows the vertical displacement around the center of drifting disturbance at different times in a reference frame moving with the basic wind. The early response of the fluid to the heating is an upward displacement at the drifting center and downward displacements to the upstream and downstream sides of the growing disturbance. The weak downward displacements are necessary to compensate for the upward motion at the center as required by the mass continuity even though that air was also heated by the wings of the pulse. Once the updraft at the drifting center weakens, the fluid in the adjacent regions can rise. By letting $\hat{x}$=0 in (104), the equation reduces to the growth function

$$\hat{\eta}_D=1-e^{-\hat{t}}. \tag{106}$$

As $\hat{t}\to\infty$, Eq. (104) becomes

$$\hat{\eta}_D(\infty,x,z)=\frac{1}{\hat{x}^2+1},\ \text{for}\ z_o-d<z<z_o+d, \tag{107}$$

which is everywhere proportional to the total amount of heat received by that air parcel. Figure 16b shows the nondimensional vertical velocity which corresponds to Fig. 16a. This is obtained by taking the time derivative of Eq. (104):

$$\hat{w}_D=\frac{1}{(\hat{x}^2+1)^2}\exp\left(\frac{-\hat{t}}{\hat{x}^2+1}\right)\left[2\,\hat{x}\sin\left(\frac{\hat{t}\,\hat{x}}{\hat{x}^2+1}\right)-(\hat{x}^2-1)\cos\left(\frac{\hat{t}\,\hat{x}}{\hat{x}^2+1}\right)\right]. \tag{108}$$

The updraft at the drifting center is accompanied by downdrafts on both sides in the early stages. At later times, two updrafts develop and propagate outward. This is analogous to the left and right moving waves in a two-dimensional shallow water system. These updrafts will overcome the downward displacement produced earlier and generate upward displacement at later times, as can be seen from Fig. 16a. At this time, the original disturbance has split in two.

For the flow response at the origin of the initial heating, the solution can be obtained by setting x=0 in $\hat{x}$ in (104). The nondimensional form of the vertical displacement can be written as

$$\hat{\eta}_o=\frac{1}{(\hat{t}^2+1)}\left\{1-\exp\left(\frac{-\hat{t}}{F(\hat{t}^2+1)}\right)\left[\hat{t}\sin\left(\frac{\hat{t}^2}{F(\hat{t}^2+1)}\right)\right.\right.$$

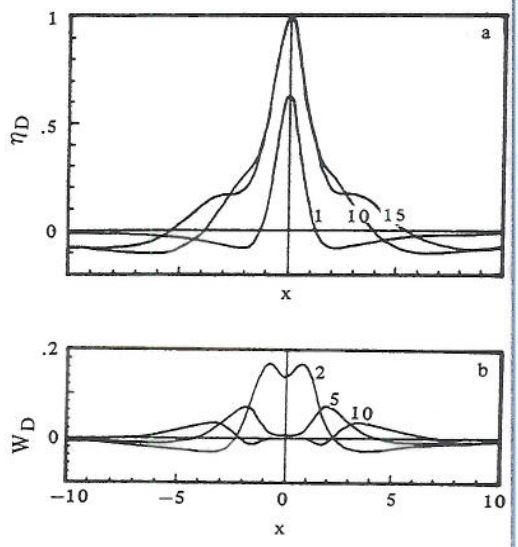

Fig. 16. (a) The vertical displacement at the center of the pulse heat source in a reference frame moving with the basic flow. The solution is given by Eq. (104). Notice that the strong updraft at the drifting center is accompanied by weak downdrafts on both sides. (b) The vertical velocity corresponding to (a). The numbers indicate the nondimensional times. (From Lin and Smith, 1986)

$$+\cos\left(\frac{\hat{t}^2}{F(\hat{t}^2+1)}\right)]\}, \qquad (109)$$

where F is the Froude number associated with the thermal forcing, defined as U/Nd. A similar number has been used by Thorpe *et al.* (1980). Notice that the response of the flow at x=0 is strongly dependent on F and changes sign at $F=1/n\pi$. With a shallow heating, the Froude number is always greater than $1/\pi$. Thus, the vertical displacements near the origin of the heating have the same sign. Equation (109) indicates that $\hat{\eta}_o$ decays as $1/\hat{t}$ as $\hat{t}\to\infty$ (Fig. 17). The response of the flow at the origin of pulse heating is an upward displacement followed by a downward displacement, as the heated air drifts away. The downward displacement produced at later times is associated with the compensating downdraft as the growing updraft drifts downstream. Raymond (1986) has investigated the flow response to a prescribed steady heat source for a wide variety of Froude numbers.

2. Flow Response to a Steady Heating

As mentioned earlier, studies of steady heating in a moving atmosphere in connection to orographic rain (Smith and Lin, 1982), heat islands (Fig. 22; Garstang *et al.*, 1975; Mahrer and Pielke, 1976) and thunderstorm downdrafts (Thorpe *et al.*, 1980) showed a curious negative relationship between heating and vertical displacement. That is, a downward (upward) displacement in the vicinity of the heat source (sink) is produced by the heating (cooling). This result is directly related to the steadiness of the heating (Lin and Smith, 1986; Bretherton, 1988) and will be explained below.

The vertical displacement of a moving stratified fluid to a pulse of point heat source may be obtained by taking $b\to 0$ and keeping bQ_o constant in Eq. (102):

$$\eta(t,x,z)=\frac{-q_o t}{2\pi N X^2}\cos\left(\frac{N z t}{X}\right), \qquad (110)$$

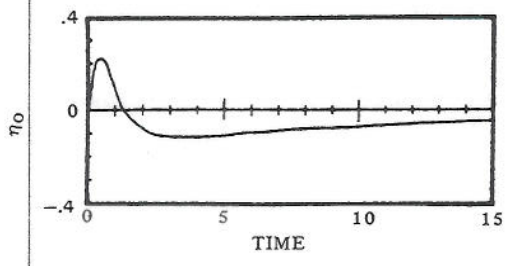

Fig. 17. The time evolution of nondimensional vertical displacement at the origin of the pulse heating. The solution is given by Eq. (109). The response is an upward displacement followed by a downward displacement, as the heated air drifts away. (From Lin and Smith, 1986)

where $q_o = bQ_o$, and $X = (x - Ut)/b$. The above equation is identical to Eq. (3) of Bretherton (1988). Figure 18 shows the vertical displacement at time t after a localized impulsive buoyancy source is imposed at t=0 in a stratified fluid. Since we are interested in the response near the origin of the heating (x=z=0), the above equation reduces to

$$\eta(t,0,0)=\frac{-q_o}{2\pi N U^2 t}. \qquad (111)$$

The steady state heat source may be regarded as a succession of very short heat pulses. Thus, the vertical displacement at the origin of the heating can be obtained by the Green's function method, which amounts to integrating Eq. (111) with respect to time:

$$\eta(t,0,0)=\int_0^t \eta(t-\tau,0,0)\,d\tau=\int_0^t \eta(T)\,dT$$

$$\mathrm{E}\int_{\Delta x/U}^{t}\eta(T)\,dT=\frac{-q_o}{2\pi N U^2}\ln\left(\frac{tU}{\Delta x}\right), \qquad (112)$$

where Δx is a characteristic horizontal distance such that $\Delta x < Ut$. The contribution to the displacement from times less than $\Delta x/U$ is assumed to be negligible (Bretherton, 1988). Therefore, the vertical displacement grows logarithmically and negatively at the origin of the heat source. The vertical displacement for the steady heating, which is distributed horizontally and

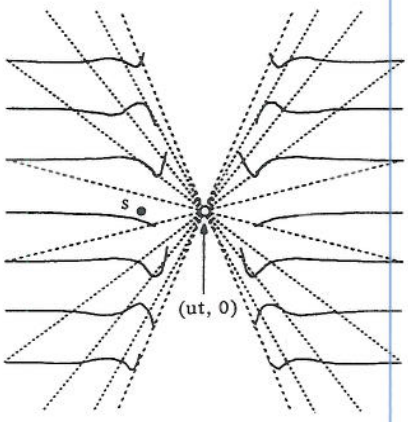

Fig. 18. The vertical displacement at time t after a localized impulsive buoyancy source is imposed at t=0 in a stratified fluid. The dashed lines are the nodal lines $z=(n+1/2)\pi X/Nt$ on which there is no vertical displacement. The solid lines are dye lines that were initially horizontal and have been displaced in response to the source. (From Bretherton, 1988).

vertically, can also be obtained by integrating Eq. (103) with respect to time.

An alternative way to explain this phenomenon is by considering the energy budget. The linearized steady state energy equation may be derived by introducing the relation, $\theta'/\theta_o \sim -\rho'/\rho_o$, (which may be obtained by linearization and combination of Poisson's equation and the equation of state for an ideal gas) in Eq. (16) and excluding the basic shear terms,

$$\frac{\partial}{\partial x}(EU+p'u')+\frac{\partial}{\partial z}(p'w')=-\frac{g^2}{c_p T_o N^2}\rho' q', \quad \textbf{(113)}$$

where $E=0.5\rho[u'^2+(g\rho'/N\rho_o)^2]$ is the perturbation wave energy in a hydrostatic atmosphere. According to the above equation, in order to add the thermal energy to the system, the steady heating must be added where the air density is low, i.e., at high temperature. This implies that the perturbation flow field must adjust itself so that the regions of negative density anomaly (negative displacement) receive the heat.

Using a group velocity argument, Bretherton (1988) showed that the t^{-1} dependence of η is a geometrical effect, which relies only on the fact that there are wavenumbers with zero group velocity around which there is a finite rate of dispersion. The small, but nonzero, group velocities of nearby wavenumbers spread their energy into a region of space that expands linearly with time in each direction, so that the energy density, a quadratic function of η, decreases as t^{-2}. The vertical displacement of the fluid to a maintained heat source grows logarithmically since the displacements produced by individual heat pulses are all in phase at the origin of the heating. Notice that the waves of zero group velocity also have zero frequency.

Since the vertical displacement grows logarithmically near the origin of the steady heat source, the flow must undergo a permanent change, instead of being a localized steady state response. As discussed by Smith and Lin (1982), this is due to the fact that a net amount of heat has been received by the airstream. To avoid this net heating problem, Smith and Lin have shown that a steady state response will occur if the horizontally integrated heating is zero. Bretherton (1988) extended Smith and Lin's result to a more general criterion. He proved that if a steady buoyancy source $q'(x, z)$ is turned on at $t=0$, then a finite, steady displacement field $\eta(x, z)$ will set up only when

$$\int_{-\infty}^{\infty} q'(x,z)\, e^{\pm iNz/U}\, dx\, dz = 0. \quad \textbf{(114)}$$

That is, when there is no projection of the heat source on the wavenumbers $\pm\boldsymbol{k}_o=(0, \pm N/U)$ corresponding to the ω^+ and ω^- modes which have zero group velocity. The $\omega^{\pm}$ modes denote the internal gravity waves which have frequencies of $Uk\pm Nk/m$ and group velocities of $\boldsymbol{c}_g^{\pm}(\boldsymbol{k})=(U\pm N/m, -Nk/m^2)$.

The gravity waves produced by a pulse heating in an unsheared flow are symmetric about its center and impart no net momentum flux to the flow. Thus, no vertically propagating gravity waves are produced. However, vertically propagating gravity waves can be generated by steady heating or cooling. Similar to Eq. (112), the vertical displacement for the steady state heating can be obtained by integrating Eq. (103) with respect to time:

$$\eta(t,x,z)=\int_0^t \eta(t-\tau,x,z)\, d\tau. \quad \textbf{(115)}$$

Figure 19 shows an example in which a heat source concentrated in the stippled region is given by a Heaviside function at $t=0$ in an unbounded stratified fluid. The solution is given by Eqs. (115) and (103) by excluding the lower boundary reflections (i.e., the last two terms in (103)). The integrand in Eq. (115) is computed numerically using Simpson's rule. The response of the fluid has two separate parts. First, there exists a region of upward displacement generated initially at the origin of the heat source and which is subsequently ad-

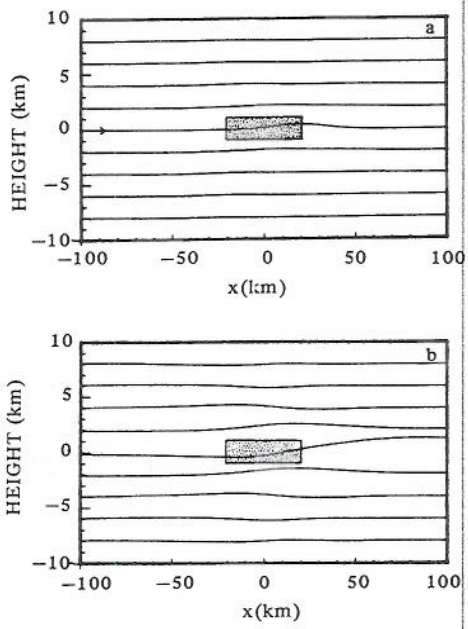

Fig. 19. Vertical displacement of a hydrostatic atmosphere to a steady heating (stippled) imposed at $t=0$. The solution is given by Eqs. (115) and (103), excluding the lower boundary reflections (the last two terms), with $U=10$ ms^{-1}, $N=0.01$ s^{-1}, $T_o=273$ K, $Q_o=1$ J kg^{-1} s^{-1}, $b=20$ km, $d=1$ km, and $z_o=0$ km. (From Lin and Smith, 1986)

vected downstream by the basic wind. The amplitude of the displacements keeps growing with time. Notice that the peak of the upward displacement appears to propagate downstream with a slower speed (~0.7U) than the basic flow. The upward displacement is a superposition of an infinite number of individual elements corresponding to individual pulse heating separated by infinitesimal time intervals. In addition, there is a downward displacement in the vicinity of the stationary source, which develops at a much slower rate than that of the drifting disturbance. The corresponding vertical momentum fluxes are shown in Fig. 20. There exists a layer of negative (positive) momentum flux above (below) the heating layer. The magnitude of the momentum flux increases as the gravity wave associated with the steady heating becomes stronger and propagates to higher (lower) layers. In the upper layer, the downward transport of momentum is a consequence of the upstream phase tilt of the vertical displacement, which gives a greater horizontal perturbation velocity in the downward motion. This is similar to the mountain wave theory (Eliassen and Palm, 1960). The convergence of momentum flux at the heating level must act to accelerate the flow slowly (as a second-order quantity) there while air above and below is decelerated.

3. Applications

A. Flow over a Heat Island

The above theory has been applied to the problem of stratified flow over a heat island by Lin and Smith (1986). This helps to explain the downward displacement observed over a heated island and upward displacement on the downstream side (Fig. 22; Malkus, 1963; Garstang *et al.*, 1975). Figure 21 shows the disturbance generated by a stationary heat source (stippled region) introduced at an initial time, t=0, in a hydrostatic atmosphere over a flat surface. The heating represents the low-level sensible heating caused by a heated island in the daytime. For the heating rate, we consider a simple case of a heat island which warms 10 K from 0600 to 1400 LST. For simplicity, we assume that the heating extends uniformly to the top of the boundary layer, say 1 km. The heat flux thus calculated is approximately 348 J m^2 s^{-1}. This gives a heating rate of 0.35 J kg^{-1} s^{-1}. The response of the fluid to the low-level heating is similar to the case in Fig. 19 in that heating correlates with negative displacement. The dynamics are essentially the same as explained in Section IV.2. Notice that the air parcel ascends on the downwind side of the heat island. Figure 22 shows the divergence and vertical velocity fields over Barbados (DeSouza, 1972; summarized in Garstang *et al.*, 1975), which indicates that there exists a downward motion over the island and an upward motion downwind during the day. Rainfall enhancement is often observed on the downwind side of metropolitan areas, such as St. Louis (Fig. 1; Braham and Dungey, 1978; Changnon, 1981). This phenomenon is often explained by the addition of condensation nuclei, which are swept downstream when air flows past an urban heat island. A

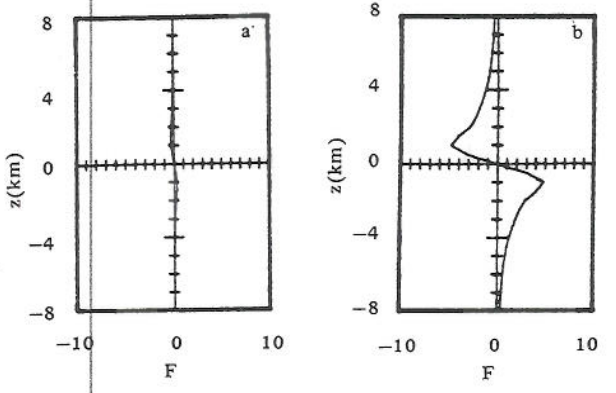

Fig. 20. The corresponding vertical momentum fluxes for the flow fields of Fig. 19. The units of the momentum flux are 10^4 Newton m^{-1}.

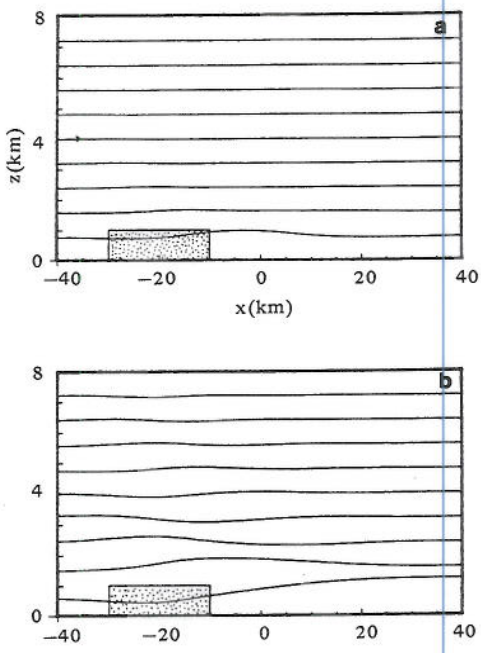

Fig. 21. Vertical displacement for an airflow over a heat island. The stationary heat source is concentrated in the stippled region. This flow is given by Eq. (115) with U=5 ms^{-1}, N=0.01 s^{-1}, T_o=273 K, Q_o=0.35 J kg^{-1} s^{-1}, z_o=0.5 km, b=10 km, d=0.5 km and c=20 km. Two times are shown: (a) 5000 s and (b) 20000 s. (From Lin and Smith, 1986)

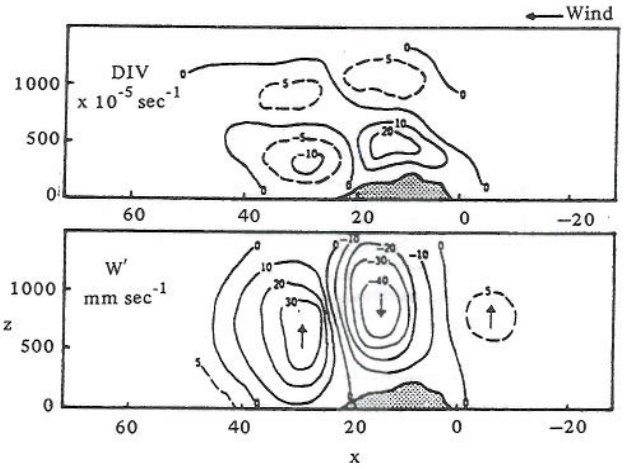

Fig. 22. Divergence and vertical velocity fields over Barbados during the summers of 1968 and 1969 during the day. The horizontal and vertical distance units are in km and m, respectively. (From Garstang *et al.*, 1975, after DeSouza, 1972)

study of the combined effects of the addition of condensation nuclei in the region of ascending motion downstream of an urban heat island may provide a better explanation of the phenomenon. A similar phenomenon has also been obtained in linear studies by Hsu (1987b) and Luthi *et al.* (1989) and in the nonlinear numerical study by Hjelmfelt (1982).

B. Orographic Rain

Figure 23 shows an example in which the heating is associated with a stationary precipitating upslope orographic cloud in a hydrostatic atmosphere. The solution is obtained by superimposing the mountain induced wave (Eq. (80c)) and the heat induced wave (Eq. (115)). The dry mountain wave solution is also plotted for comparison. The heating rate corresponds to a rainfall rate of about 2.5 mm h^{-1}. The heating is concentrated in the stippled region and activated at t=0 s. After some time, the thermally generated disturbance has grown and drifted downstream. This displacement keeps growing as the stationary heating continues and reaches considerable magnitude by 13,000 s≈3.6 hrs (Fig. 23b). If the heating continues for some time, a negative dis placement is produced in the vicinity of the upslope orographic cloud. This phenomenon was found by Smith and Lin (1982) and is explained more completely here. In the real atmosphere, broad upslope rain may be limited by the heat induced descent either in duration or intensity. This result has some similarities to a number of studies of mountain waves and orographic rain (e.g., Raymond, 1972; Fraser *et al.*, 1973; Barcilon *et al.*, 1980). The vertical transport of the horizontal momentum is convergent at the heating layer, which is similar to the case of an unbounded fluid (Fig. 20)

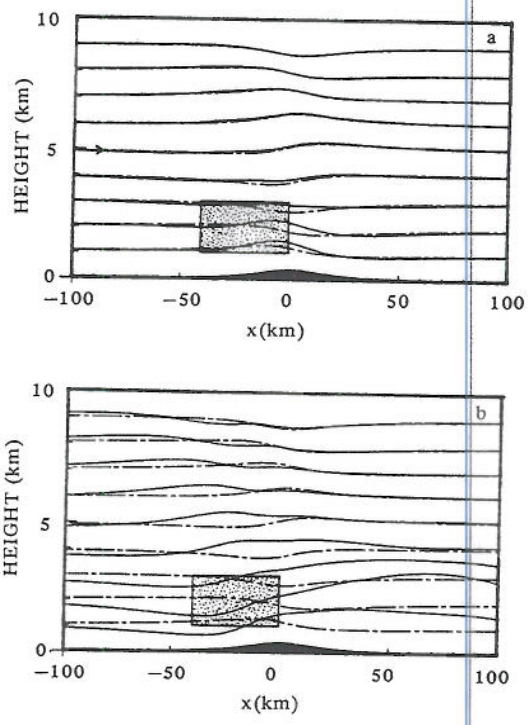

Fig. 23. Hydrostatic vertical displacement generated by a mountain and an elevated heat source (stippled) imposed at t=0. The solution is given by Eqs. (80c), (103) and (115) with U=10 ms^{-1}, N=0.01 s^{-1}, T_o=273 K, Q_o=1 J kg^{-1} s^{-1}, b=20 km, d=1 km and c=20 km, a=20 km, h_o=400 m. The dashed lines represent the vertical displacement of the adiabatic mountain waves. Two times are shown: (a) 3000 s and (b) 13000 s. The heating corresponds to a precipitation of 2.5 mm h^{-1}. (From Lin and Smith, 1986)

with the modification of orographic effects. With certain realistic values of the parameters U, N, Q_o, b, d, and z_o, a positive momentum flux below the heating layer is produced, implying a reverse of the mountain drag as discussed in Smith and Lin (1982) and Durran and Klemp (1982).

To avoid the addition of latent heat in a region of downward motion, Lin (1986b) adopted a simple rain parameterization in a linear, finite-element numerical model. The diabatic heating is parameterized by

$$q' = \left(\frac{c_p T_o N^2}{g}\right) \varepsilon w' \alpha(w, \eta), \qquad \textbf{(116)}$$

where

$$\varepsilon = 1 - \frac{N_w^2}{N^2},\ N^2 = \frac{g}{T_o}(\Gamma_d - \Gamma),\ N_w^2 = \frac{g}{T_o}(\Gamma_s - \Gamma),$$

$$\alpha(w, \eta) = 1 \quad \text{if } w > 0 \text{ and } \eta > 0,$$

$$\alpha(w,\eta)=0 \quad \text{otherwise.} \tag{117}$$

In the above formulation, the cloud forms immediately in a region of upward velocity and displacement and falls to the surface immediately in a region of downward velocity or displacement. This parameterization of a precipitating cloud is similar to that used by Fraser *et al.* (1973) and Barcilon *et al.* (1980). The parameter ε can be as small as 0.2 in cold air (Barcilon *et al.*, 1980). Equation (116) may be substituted into the thermodynamic equation, Eq. (13), with the terms of V, U_z and V_z excluded to obtain

$$\frac{\partial \theta'}{\partial t}+U\frac{\partial \theta'}{\partial x}+\frac{N^2\theta_o}{g}(1-\varepsilon\alpha)w'=0. \tag{118}$$

The parameter α will be greater than or equal to zero depending upon whether the point of interest is inside or outside the cloud. The air parcel follows a moist adiabat if it is inside the cloud and a dry adiabat if outside the cloud.

Figure 24 shows the numerical results of orographic rain in a stable atmosphere with ε=0.8. The stability parameter (ε) is approximately equal to an actual lapse rate of 6.25 K km^{-1} with a moist lapse rate of 7 K km^{-1}. The incoming airstream is saturated, and the moisture is limited to the lower 6 km. The parameterization is turned on at 10,000 s. Four time steps are shown to indicate the time evolution of the flow. The heating regions are outlined, which may represent the cloud boundaries. At 30,000 s, two drifting clouds appear to the downwind side of the mid- and low-level stationary clouds. These drifting clouds originate and subsequently separate from the stationary clouds. The flow reaches a steady state locally in the vicinity of the mountain at later times as shown in Fig. 24d. The local features of the low-level stationary cloud are similar to those found by Barcilon *et al.* (1980). The two stationary clouds at the lower and middle levels may be interpreted as local quasi-stationary heat sources. According to the finding of Smith and Lin (1982), the phase relationship between the stationary heating and the heat-induced vertical displacement in the flow parameters chosen here is negative. However, the orographic lifting acts to support the existence of the stationary clouds. In short, the two stationary clouds in Fig. 24d are supported by the orographic forcing and limited by the long-term heating generated by the clouds themselves. The corresponding dry mountain wave is plotted (dotted lines) against the moist flow (Fig. 24d). In general, the streamlines are depressed upstream in the lower layer (e.g., z=2 km) and lifted downstream in the middle layer (e.g., z=4 km) by the presence of moisture.

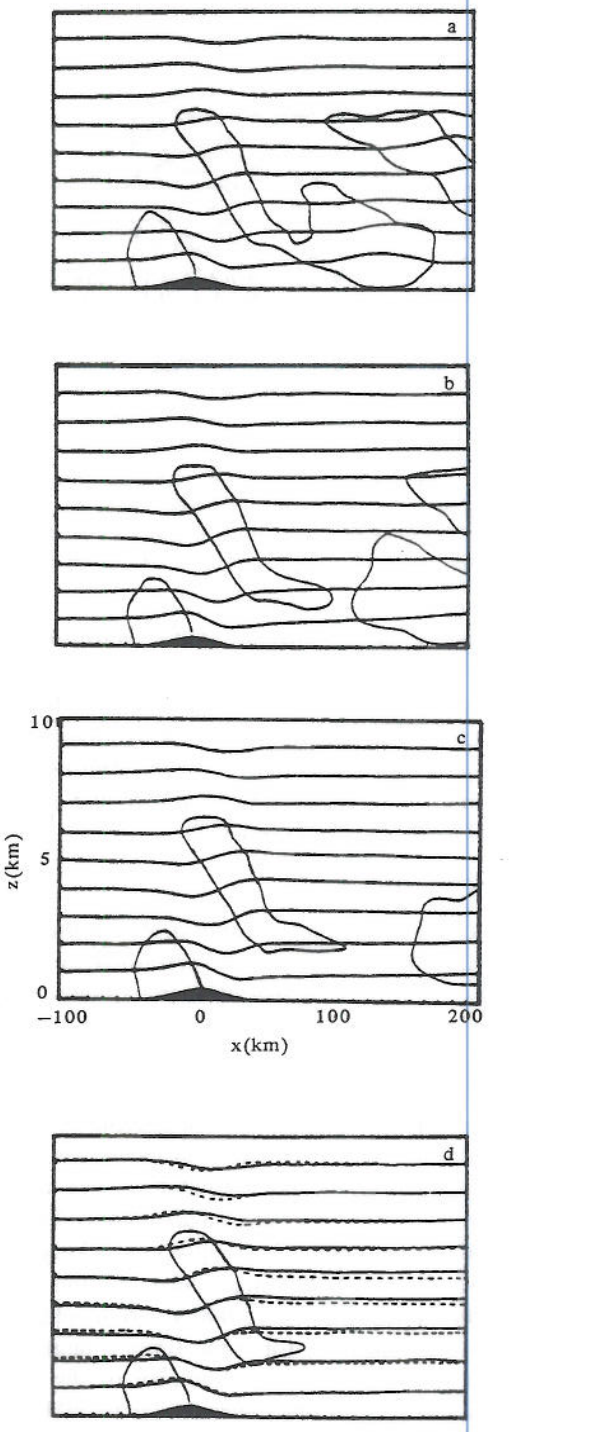

Fig. 24. Streamlines and heating regions of precipitating orographic clouds in a stable atmosphere with ε=0.8 simulated by a linear, finite element model. Other parameters of the flow are U=10 ms^{-1}, N=0.01 s^{-1}, T_o=273 K, and ρ_o=1 kg m^{-3}. The flow is directed from left to right. The mountain height and half-width are 400 m and 20 km, respectively. The dotted lines in (d) are the corresponding dry mountain waves. Four time steps are shown: (a) 30000 s, (b) 40000 s, (c) 50000 s, and (d) 60000 s. (From Lin, 1986b)

Barcilon and Fitzjarrald (1985) investigated the nonlinear effects on a precipitating orographic cloud using a theoretical approach and a rain parameterization similar to that of Eq. (116). They found that the nonlinearity and lower boundary affects the dynamics of mechanically and thermally induced waves and wave drag. The wave drag depends upon: (1) the location of the moist layer with respect to the ground, (2) the amount of moisture, (3) the degree of nonlinearity and (4) the asymmetry in the bottom topography. For symmetrical mountain profiles, substantial drag reductions are obtained when the moisture is adjacent to the topography. In addition, an increase in the nonlinearity increases the drag.

C. Moist Convection

The maintenance of a quasi-steady squall line remains an unsolved dynamical problem. One may regard the evaporative cooling in the subcloud layer produced by the precipitation falling from the updraft aloft as a stationary heat sink in the reference frame of the moving line. The steady state assumption for the cooling in a squall-line type of thunderstorm is not an unreasonable one (Lilly, 1979). Figure 25 shows an example of an airflow over a stationary heat sink. In a moving frame, the stationary heat sink may be regarded as a left-moving squall line. The propagation speed of the heat sink is 15 ms^{-1}, and the Froude number (U/Nd) is 1.5. In the vicinity of the heat sink, the air is displaced downward at first and then upward. The approach to steady state is essentially the same as in the flow over a heat source but in an opposite way. The local features near the heat sink are similar to the steady state solutions of Thorpe *et al.* (1980) and Lin and Smith (1986). The phase relationship between the evaporative cooling and the induced vertical displacement in the region near the heat sink is negative, as shown earlier. The upstream tilt of the vertical displacement indicates the upward propagation of the generated internal gravity waves. In addition, there is a region of positive displacement propagating downstream kinematically, which is similar to the heating case studied earlier.

The positive displacement in the vicinity of the heat sink resembles the flow structure near the gust front of a squall line and may provide a possible mechanism for the maintenance of a squall line. Robustness of this result can be demonstrated by solving the same problem with a linear finite-element numerical model (Lin, 1986b). This is also a convenient way to exhibit other aspects of the flow field as all of the flow variables are computed by the model. Figure 26 shows the vertical displacement, perturbation fields of the density, horizontal velocity and vertical velocity at 4000 s.

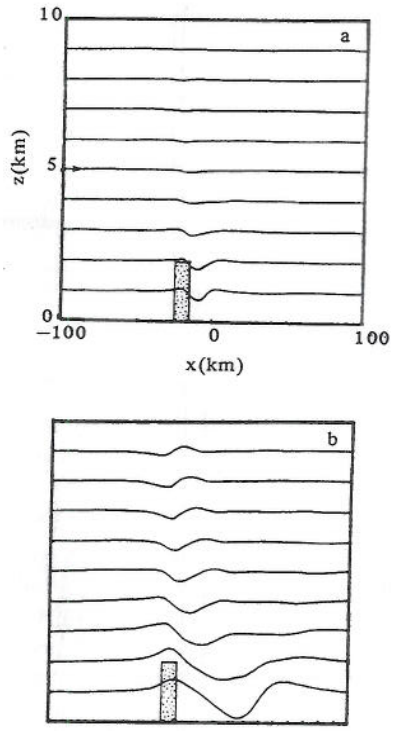

Fig. 25. Vertical displacement near a stationary heat sink representing evaporative cooling under a precipitating cloud. This flow is given by Eqs. (115) and (103) with U=15 ms^{-1}, N=0.01 s^{-1}, Q_o=-4 J kg^{-1} s^{-1}, z_o=1 km, b=5 km, d=1 km and c=20 km. Two times are shown: (a) 1000 s and (b) 4000 s. (From Lin and Smith, 1986)

The field of vertical displacement produced by the numerical model (Fig. 26a) is slightly smoother than that of the analytical solution (Fig. 25b) because a numerical smoothing technique is applied in the model to avoid the spurious growth of high wave number modes. In general, the agreement between the numerical model and analytical results is good. The density field (Fig. 26b) shows that there exists a pool of cold air near the stationary heat sink. The sharp density difference in front of the heat sink (x = −35 km) may be regarded as an upstream gust front produced by the density current. The high density region may correspond to the mesohigh as often observed under the strong downdraft region. On the downwind side, the cold air is advected more dispersively, i.e., the density difference is not as sharp as on the upstream side . From the velocity fields (Figs. 26c, d), there exists upstream motion and a region of surface convergence in front of the stationary heat sink. This is consistent with the finding of the positive displacement near the heat sink (Fig. 25). With application to the low-level flow associated with a squall line, the upward motion and low-level convergence may play an important role in generating a new convective area on the upstream side of the moving squall line.

V. Concluding Remarks

The dynamics of mesoscale circulations of a stably stratified flow forced by both low-level and elevated heat sources or sinks have been reviewed. The mathematical problems of prescribed diabatic heating in a continuously stratified flow have been solved by several authors and have been shown to be useful in understanding the dynamics of various mesoscale phenomena which commonly occur in the terrestrial atmosphere. In this paper, we have reviewed a relatively wider variety of problems and emphasized more the basic dynamics. In part I, we discussed the responses of a stably stratified uniform flow to a prescribed thermal forcing. The governing equations, energy equation, momentum transport, dispersion relation, and various wave regimes and properties were discussed. Mathematical methods for solving both steady and transient flows over a meso-γ scale heat source were presented. The mathematical solutions have been found to be useful in helping to understand problems of heat island, orographic rain, moist convection, and gravity waves traveling on inversions.

To wholly understand the problems of orographic rain and moist convection, the present approach may be extended to include a more realistic rain parameterization or an explicit moisture budget. A more realistic boundary layer physics needs to be considered when one applies the present theory to predict the flow circulation associated with a heat island while a more realistic flow structure needs to be incorporated in the theory when one investigates the propagation mechanisms of gravity waves generated in the atmosphere. The responses in a shear flow will be reviewed in Part II.

Acknowledgments

The author wishes to express his sincere appreciation to R. B. Smith of Yale University for introducing him to mesoscale dynamics, which helped to stimulate the series of work presented in this review. Discussions with R. F. Adler, A. Barcilon, C. Bretherton, C.-S. Chen, W.-D. Chen, D. R. Durran, K. Emanuel, G. M. Heymsfield, R. Hughes, G. S. Janowitz, D. Keyser, D. J. Raymond, R. Rotunno, and W.-Y. Sun among others were very helpful. The author is grateful to R. P. Weglarz and T.-A. Wang for reading the manuscript.

References

Abdullah, A. J. (1955) The atmospheric solitary wave. *Bull. Amer. Meteor. Soc.*, **10**, 511-518.

Barcilon, A. and D. Fitzjarrald (1985) A nonlinear steady model for moist hydrostatic mountain waves. *J. Atmos. Sci.*, **42**, 58-67.

Barcilon, A., J. C. Jusem, and S. Blumsack (1980) Pseudo-adiabatic flow over a two-dimensional ridge. *Geophys. Astrophys. Fluid Dyn.*, **16**, 19-33.

Bergeron, T. (1968) Studies of the oreigenic effect on the areal fine structure of rainfall distribution. *Met. Inst. Uppsala Univ.*, Report No. **6**.

Blumen, W. and R. G. Hendl (1969) On the role of Jule heating as a source of gravity wave energy above 100 km. *J. Atmos. Sci.*, **26**, 210-217.

Booker, J. R. and F. P. Bretherton (1967) The critical layer for internal gravity waves in a shear flow. *J. Fluid Mech.*, **27**, 513-539.

Bosart, L. F. and J. P. Cussen (1973) Gravity wave phenomena accompanying east coast cyclogenesis. *Mon. Wea. Rev.*, **101**, 446-454.

Bosart, L. F. (1981) The presidents' Day snowstorm of 18-19 February 1979: A subsynoptic scale event. *Mon. Wea. Rev.*, **109**, 1542-1566.

Braham, R. R. and M. J. Dungey (1978) A study of urban effects on radar first echoes. *J. Appl. Meteor.*, **17**, 644-654.

Bretherton, C. (1988) Group velocity and the linear response of stratified fluids to internal heat or mass sources. *J. Atmos. Sci.*, **45**, 81-93.

Bretherton, F. P. (1966) The propagation of groups of internal gravity waves in a shear flow. *Quart. J. Roy. Meteor. Soc.*, **92**, 466-480.

Bretherton, F. P. (1969) Momentum transport by gravity waves. *J. Atmos. Sci.*, **45**, 81-93.

Browning, K. A., C. W. Pardoe, and F. F. Hill (1974) Structures and mechanism of precipitation and the effects of orography in a winter time warm sector. *Quart. J. Roy. Meteor. Soc.*, **100**, 309-330.

Browning, K. A. (1980) Structure, mechanism and prediction of orographically enhanced rain in Britain, in Orographic Effects in Planetary Flows, GARP Publication Series #23, WMO, Geneva.

Changnon, S. A. (1981) METROMEX: A review and summary. *Met. Monograph.*, **40**, Amer. Meteor. Soc., 181 pp.

Christie, D. R., K. J. Muirhead, and A. L. Hales (1978) On the solitary waves in the atmosphere. *J. Atmos. Sci.*, **35**, 805-825.

Davies, H. C. and C. Schar (1986) Diabatic modification of airflow over a mesoscale orographic ridge: A model study of the coupled response. *Quart. J. Roy. Meteor. Soc.*, **112**, 711-730.

DeSouza, R. L. (1972) A study of atmospheric flow over a tropical island. Master's thesis, Dept. of Meteor., Florida State Univ., 203 pp.

Durran, D. R. and J. B. Klemp (1982) The effects of moisture on trapped mountain waves. *J. Atmos. Sci.*, **39**, 2490-2506.

Eliassen, A. and E. Palm (1960) On the transfer of energy in stationary mountain waves. *Geofys. Publ.*, **22**, 1-23.

Emanuel, K. and D. J. Raymond (1984) *Dynamics of Mesoscale Weather Systems*. J. B. Klemp, Ed., 591 pp. NCAR Summer Colloquium Lecture Notes. NCAR, Boulder, U.S.A.

Ferguson, H. L. (1967) Mathematical and synoptic aspects of a small scale wave disturbance over the Lower Great Lakes. *J. Appl. Meteor.*, **6**, 523-529.

Fraser, A. B., R. Easter, and P. Hobbs (1973) A theoretical study of the flow of air and fallout of solid precipitation over mountainous terrain. *J. Atmos. Sci.*, **30**, 813-823.

Garstang, M., P. D. Tyson, and G. D. Emmitt (1975) The structure of heat islands. *Rev. Geophys. Space Phys.*, **13**, 139-165.

Geisler, J. E. and F. P. Bretherton (1969) The seabreeze forerunner. *J. Atmos. Sci.*, **26**, 82-95.

Goldstein, S. (1931) On the stability of superposed streams of fluid of different densities. *Proc. Roy. Soc. London*, **A132**, 524-548.

Gossard, E. E. and W. H. Hooke (1975) *Waves in the Atmosphere*. 456 pp. Elsevier Scientific, U.S.A.

Grimshaw, R. (1981) A second order theory for solitary waves in

deep fluids. *Phys. Fluids*, **24**, 1611-1618.

Grossman, R. L. and D. R. Durran (1984) Interaction of low-level flow with the Western Ghat Mountains and offshore convection in the summer monsoon. *Mon. Wea. Rev.*, **112**, 652-672.

Henz, J. F. (1972) An operational technique of forecasting thunderstorms along the lee slope of a mountain ridge. *J. Appl. Meteor.*, **11**, 1284-1292.

Heymsfield, G. M. and R. H. Blackmer, Jr. (1988) Statellite-observed characteristics of Midwest severe thunderstorm anvils. *Mon. Wea. Rev.*, **116**, 2200-2224.

Hildebrand, F. B. (1976) *Advanced Calculus for Applications*. 2nd ed., 733 pp. Prentice-Hall Inc., U.S.A.

Hjelmfelt, M. R. (1982) Numerical simulations of the effects of St. Louis on mesoscale boundary layer airflow and vertical air motion: Simulations of urban vs non-urban effects. *J. Appl. Meteor.*, **31**, 1239-1257.

Hobbs, P. V., R. Houze, Jr., and T. Matejka (1975) The dynamical and microphysical structure of an occluded frontal system and its modification by orography. *J. Atmos. Sci.*, **32**, 1542-1562.

Hoiland, E. (1951) Fluid flow over a corrugated bed. Fifth Prog. Rep., Contract AF19 (122)-263. Air Force Cambridge Research Center.

House, D. C. (1961) The divergence equation as related to severe thunderstorm. *Bull. Amer. Meteor. Soc.*, **42**, 803-816.

Hus, H.-M. (1987a) Study of linear steady atmospheric flow above a finite surface heating. *J. Atmos. Sci.*, **44**, 186-199.

Hus, H.-M. (1987b) Mesoscale lake-effect snowstorms in the vicinity of Lake Michigan: Linear theory and numerical simulations. *J. Atmos. Sci.*, **44**, 1019-1040.

Hunt, J. N., R. Palmer, and W. Penney (1960) Atmospheric waves caused by large explosions. *Phil. Trans. Roy. Soc., London*, **A252**, 275-315.

Kaplan, M. L. and D. A. Paine (1977) The observed divergence of the horizontal velocity field and pressure gradient force at the mesoscale: Its implications for the parameterization of three-dimensional momentum transport in synoptic-scale numerical models. *Beitr. Phys. Atmos.*, **50**, 321-330.

Koch, S. E. and P. B. Dorian (1988) A mesoscale gravity wave event observed during CCOPE. Part III: Wave environment and probable source mechanisms. *Mon. Wea. Rev.*, **116**, 2570-2592.

Lamb, H. (1932) *Hydrodynamics*. 738pp. Dover Publications, 6th Ed., U.S.A.

LeBlond, P. H. and L. A. Mysak (1978) *Waves in the Ocean*. 602pp. Elsevier Scientific, U.S.A.

Lilly, D. K. (1979) The dynamical structure and evolution of thunderstorms and squall lines. *Ann. Rev. Earth Planet. Sci.*, **7**, 117-161.

Lin, C. A. and R. E. Stewart (1991) Diabatically forced mesoscale circulations in the atmosphere. *Adv. Geophys.*, **33**, B. Saltzman, Ed. Academic Press, NY, 267-305.

Lin, C. A., K. K. Szeto, and R. E. Stewart (1988a) Mesoscale circulations forced by melting snow. Part I: Basic simulations and dynamics. *J. Atmos. Sci.*, **45**, 1629-1641.

Lin, C. A., R. E. Stewart, and K. K. Szeto (1988b) Mesoscale circulations forced by melting snow. Part II: Application to meteorological features. *J. Atmos. Sci.*, **45**, 1642-1650.

Lin, Y.-L. (1986a) Calculation of airflow over an isolated heat source with application to the dynamics of V-shaped clouds. *J. Atmos. Sci.*, **43**, 2736-2751.

Lin, Y.-L. (1986b) A study of the transient dynamics of orographic rain. *Pap. Meteor. Res.*, **9**, 19-45.

Lin, Y.-L. (1987) Two-dimensional response of a stably stratified flow to diabatic heating. *J. Atmos. Sci.*, **44**, 1375-1393.

Lin, Y.-L. and H.-Y. Chun (1991) Effects of diabatic cooling in a shear flow with a critical level. *J. Atmos. Sci.*, **48**, 2476-2491.

Lin, Y.-L. and R. C. Goff (1988) A study of a mesoscale solitary wave in the atmosphere originating near a region of deep convection. *J. Atmos. Sci.*, **45**, 194-205.

Lin, Y.-L. and S. Li (1988) Three-dimensional response of a shear flow to elevated heating. *J. Atmos. Sci.*, **45**, 2987-3002.

Lin, Y.-L. and R. B. Smith (1986) Transient dynamics of air flow near a local heat source. *J. Atmos. Sci.*, **43**, 40-49.

Lindzen, R. S. and K. -K. Tung (1976) Banded convective activity and ducted gravity waves. *Mon. Wea. Rev.*, **104**, 1602-1617.

Luthi, D., C. Schar, and H. C. Davies (1989) On the atmospheric response to steady mesoscale low-level diabatic heating. *Contri. Atmos. Phys.*, **62**, 126-150.

Mahrer, Y. and R. A. Pielke (1976) Numerical simulation of the airflow over Barbados. *Mon. Wea. Rev.*, **104**, 1392-1402.

Malkus, J. S. (1963) Tropical rain induced by a small natural heat source. *J. Appl. Meteor.*, **2**, 547-556.

Malkus, J. S. and M. E. Stern (1953) The flow of a stable atmosphere over a heat island. Part. I. *J. Meteor.*, **10**, 30-41.

Marwitz, J. D. (1980) The structure and motion of severe hail-storms. Part I: Supercell storms. *J. Appl. Meteor.*, **19**, 913-926.

Nicholls, M. E., R. A. Pielke, and W. R. Cotton (1991) Thermally forced gravity waves in an atmosphere at rest. *J. Atmos. Sci.*, **48**, 1869-1884.

Olfe, D. B. and R. L. Lee (1971) Linearized calculation of urban heat island convection effects. *J. Atmos. Sci.*, **28**, 1374-1388.

Ogura, Y. and M.-T. Liou (1980) The structure of a midlatitude squall line: A case study. *J. Atmos. Sci.*, **37**, 553-567.

Ogura, Y. and M. Yoshizaki (1988) Numerical study of orographic-convective precipitation over the eastern Arabian Sea and the Ghat mountains during the summer monsson. *Mon. Wea. Rev.*, **45**, 2097-2122.

Orlanski, I. (1975) A rational subdivision of scales for atmospheric processes. *Bull. Amer. Meteor. Soc.*, **56**, 527-530.

Palm, E. (1953) On formation of surface waves. *Astrophys. Norvegica*, **5**(3), 1-29.

Pecnick, M. J. and J. A. Young (1984) Mechanics of a strong subsynoptic gravity wave deduced from satellite and surface observations. *J. Atmos. Sci.*, **41**, 1850-1862.

Pekeris, C. L. (1984) The propagation of a pulse in the atmosphere. Part II. *Phys. Rev.*, **73**, 145-154.

Queney, P. (1947) Upstream effects of mesoscale mountains. Dept. Meteor., Univ. of Chicago, Misc. Report No. 23, 81pp.

Queney, P. (1954) Initial value problems in a double Couette-flow. Autobarotropic Flow Project, Sci. Rep. No. 1, Contract AF19(604)-728. Air Force Cambridge Research Center.

Queney, P., G. A. Corby, N. Gerbier, H. Koschmieder, and J. Zierep (1960) The airflow over mountains. WMO Tech. Note, No. **34**, Ed. Alaka.

Raymond, D. J. (1972) Calculation of airflow over an arbitrary ridge including diabatic heating and cooling. *J. Atmos. Sci.*, **29**, 837-843.

Raymond, D. J. (1983) Wave-CISK in mass flux form. *J. Atmos. Sci.*, **40**, 2561-2572.

Raymond, D. J. (1984) A wave-CISK model of squall lines. *J. Atmos. Sci.*, **41**, 1946-1958.

Raymond, D. J. (1986) Prescribed heating of a stratified atmosphere as a model for moist convection. *J. Atmos. Sci.*, **43**, 1011-1111.

Raymond, D. J. and R. Rotunno (1989) Response of a stably stratified flow to cooling. *J. Atmos. Sci.*, **46**, 2830-2837.

Robichaud, A. and C.A. Lin (1989) Simple models of diabatically forced mesoscale circulations and a mechanism for amplification. *J. Geophys. Res.*, **94**, 3413-3426.

Rotunno, R. (1983) On the linear theory of the land- and sea-breeze.

J. Atmos. Sci., **40**, 1999-2005.
Rotunno, R., J. B. Klemp, and M. L. Weisman (1988) A theory for strong, long-lived squall lines. *J. Atmos. Sci.*, **45**, 463-485.
Sarker, R. P. (1967) Some modifications in a dynamical model of orographic rainfall. *Mon. Wea. Rev.*, **95**, 673-684.
Scorer, R. S. (1950) The dispersion of a pressure pulse in the atmosphere. *Proc. Roy. Soc., London*, **A201**, 137-157.
Scorer, R. S. (1954) Theory of airflow over mountains: III-airstream characteristics. *Quart. J. Roy. Meteor. Soc.*, **80**, 417-428.
Smith, R. C. (1955) Theory of air flow over a heated land mass. *Q. J. Roy. Meteor. Soc.*, **81**, 382-395.
Smith, R. C. (1957) Air motion over a heated land mass. Part II. *Quart. J. Roy. Meteor. Soc.*, **83**, 248-256.
Smith, R. B. (1979) The influence of mountains on the atmosphere. *Adv. in Geophys.*, **21**, Ed. B. Saltzman, Academic Press, NY, 87-230.
Smith, R. B. (1982) A differential advection model of orographic rain. *Mon. Wea. Rev.*, **110**, 306-309.
Smith, R. B. (1985) Comment on "Interaction of low-level flow with the Western Ghat Mountains and offshore convection in the summer monsoon", *Mon. Wea. Rev.*, **113**, 2176-2177.
Smith, R. B. and Y.-L. Lin (1982) The addition of heat to a stratified airstream with application to the dynamics of orographic rain. *Quart. J. Roy. Meteor. Soc.*, **108**, 353-378.
Smith, R. B. and Y.-L. Lin (1983) Orographic rain on the Western Ghats. *Mountain Meteorology*, Eds. E. R. Reiter *et al.*, pp. 71-94. *Sci. Press and Amer. Meteor. Soc.*, U.S.A.
Stobie, J. G., F. Einaudi, and L. W. Uccellini (1983) A case study of gravity waves-convective storms interaction: 9 May 1979. *J. Atmos. Sci.*, **40**, 2804-2830.
Spiegel, E. A. and G. Veronis (1960) On the Boussinesq approximation for a compressible fluid. *Astrophys. J.*, **131**, 442-447.
Taylor, G. I. (1931) Effect of variation of density on the stability of superposed streams of fluid. *Proc. Roy. Soc. London*, **A132**, 499-523.
Thorpe, A. J., M. J. Miller, and M. W. Moncrieff (1980) Dynamical models of two-dimensional downdraughts. *Quart. J. Roy. Meteor. Soc.*, **106**, 463-484.
Thorpe, A. J., M. J. Miller, and M. W. Moncrieff (1982) Two-dimensional convection in nonconstant shear: A model of mid-latitude squall lines. *Quart. J. Roy. Meteor. Soc.*, **108**, 739-762.
Uccellini, L. W. and S. E. Koch (1987) The synoptic setting and possible energy sources for mesoscale wave disturbances. *Mon. Wea. Rev.*, **115**, 721-729.
Uccellini, L. W., P. J. Kocin, R. A. Peterson, C. H. Wash, and K. F. Brill (1984) The Presidents' Day cyclone of 18-19 February 1979: Synoptic overview and analysis. *Mon. Wea. Rev.*, **112**, 31-55.
Wagner, J. A. (1962) Gravity wave over New England, 12 April 1961. *Mon. Wea. Rev.*, **90**, 431-436.
Weston, V. H. (1962) Gravity and acoustical waves. *Can. J. Phys.*, **40**, 446-452.

由熱力作用下所引發的中尺度環流的動力現象
第一部份：在無風切氣流場的反應

林玉郎

美國北卡羅來納州立大學
海洋、地球與大氣科學系

摘　要

在本文裡，我們將綜覽低層及離地熱源引發的穩定成層氣流之中尺度環流的動力基礎。連續成層氣流對固定熱源的反應之數學問題，有些已被解過，這些解對了解一些中尺度現象有所助益。在文內，我們將討論較爲廣泛的中尺度問題，討論的重點將集中在基本動力上。

在第一部份裡，我們將敍述穩定成層無風切氣流對固定熱源的反應及數學解。一些相關的控制方程、能量方程、動量傳播、頻散關係及波的特性也會被討論到。有關氣流對中小尺度熱源的穩定態及非穩定態之數學解將被詳細敍述。然後這些解將被應用到熱島、地形雨、濕對流及沿逆溫層傳播之重力波等問題上。